We are IntechOpen, the world's leading publisher of Open Access books Built by scientists, for scientists

4,800
Open access books available

122,000
International authors and editors

135M
Downloads

Our authors are among the

154
Countries delivered to

TOP 1%
most cited scientists

12.2%
Contributors from top 500 universities

WEB OF SCIENCE™

Selection of our books indexed in the Book Citation Index in Web of Science™ Core Collection (BKCI)

Interested in publishing with us?
Contact book.department@intechopen.com

Numbers displayed above are based on latest data collected.
For more information visit www.intechopen.com

7

Cathodoluminescence from Amorphous and Nanocrystalline Nitride Thin Films Doped with Rare Earth and Transition Metals

Muhammad Maqbool[1], Wojciech M. Jadwisienczak[2] and Martin E. Kordesch[2]
[1]*Ball State University*
[2]*Ohio University*
USA

1. Introduction

Rare earth (RE) ion luminescence has long been used in laser and optical fiber communications technology. Bulk RE doped oxides were widely used in color phosphors for Cathode Ray Tubes. The wide band gap (WBG) semiconductors and insulators have been used for visible emission at 300 K from RE ions since the reports first by Zanata (Zanatta and Nunes 1998) for Er in silicon nitride (photoluminescence) and then shortly thereafter by Steckl (Steckl and Birkhahn 1998) for Er in GaN. The III-nitrides were emerging as Light Emitting Diodes and semiconductors at the time, and it was reported that the luminescence intensity of the RE ions was improved by a wide band gap host. Silicon (band gap ≈ 1.1 eV) is not suited for most visible RE ion emission. Glasses and oxides were used for the infra red (IR), especially for the emission from Er^{3+} ion at ~ 1.5 μm. In 1998, RE ion incorporation into a crystalline host was often accomplished by ion implantation at low atomic concentrations, or by in situ doping (again with low atomic percentages) of the RE ions. It was believed that the quality of the host lattice was essential to the RE luminescence. However, Zanata and Nunes observed green room temperature luminescence from an Er-doped silicon nitride film deposited by reactive sputtering in nitrogen. Visible emission was observed with an estimated 10 at. % dopant concentration in an amorphous material. Both the amorphous and crystalline hosts discovered by the Zanata and Steckl groups set in motion the (enduring) pursuit of practical visible light emission devices using RE ions in wide band gap materials.

In 1999, Gurumurugan (Gurumurugan, Chen et al. 1999) sputter deposited amorphous AlN doped with Er (3.4 at.%) and observed the full range of Er emission lines in cathodoluminescence (CL) in amorphous AlN. There is no visible defect band in the large gap of AlN (~6 eV), in contrast to sputtered GaN which suffers from an intense, broad yellow emission from defects. The AlN band gap is almost identical with the crystalline AlN bandgap, and the bandgap was not reduced significantly by the RE dopant. The AlN film was transparent, amorphous, and could be deposited at 300 K. Gurumarugan et al. also showed that the amorphous AlN films could be heated to 1300 K without crystallization. The heating improved the RE emission intensity. Also, it was noted that in these films the intensity of some

of the Er^{3+} transitions *decreased* with rising temperature, and some *increased* with rising temperature.

The crystalline III-nitrides are now extensively used for LED's, lasers and solid state lighting, high power electronic devices and other passive electronics uses related to the thermal conductivity of AlN. The light emission from direct transitions in GaN and In-Al-Ga-N alloys has displaced the III-nitride RE devices in lighting applications. The low intensity and long lifetime of the RE^{3+} transitions have also hindered the application of RE luminescence for on-chip communications. Thin film materials doped with RE's are used for phosphors, and specialty applications such as in situ thermometry.

2. Growth, doping and measurement techniques

2.1 Sputter deposition

Radio frequency (RF) sputtering is a physical vapour deposition process that uses RF excitation to cause gas molecules to collide with a target, removing the target material by the mechanical impact of the sputtering gas. The RF sputtering process is well known and used for many industrial applications. The details can be obtained from several textbooks. RF magnetron sputtering is a variation most often used for the efficient deposition of thin films.

In the sputtering process, a target of a metal or insulator might be made from solid material or pressed powders. The sputter gas used is often Argon (Ar). The gas pressure is adjusted so that a plasma of Ar ions is created by the RF field above the target. In magnetron sputtering, a system of magnets is used to confine the RF field and the ions so that the target is used efficiently. In this example, the sputter gas is inert, and physically collides with the target surface to eject a target atom that is then condensed onto the substrate. In this simple example, the kinetic energy of the Ar ion is used to eject the target atom. No reaction takes place, and ideally the condensed film is composed only of the target atoms. For AlN or GaN, sputterd with Ar, the condensed film is ideally a stoichiometric film of AlN or GaN. Sputtered films are often disordered, because the process does not generate or require the input of large amounts of heat such as thermal evaporation or chemical vapor deposition. The substrate can be cold. As a consequence, the condensed atoms do not have sufficient energy on the substrate to organize into a crystalline lattice.

In reactive sputtering, the target material is sputtered in a reactive gas. The RF plasma creates ions of the reactive gas, so that impact with the target results in a compound of the target and sputter gas formed by a chemical reaction which then condenses onto the substrate. For nitrogen and aluminium, for example, the nitrogen decomposes into N ions, and reacts with the Al metal target to form AlN. For simple compounds, where there are few alternative compositions and structures, the stoichiometric product is often the most likely compound to be deposited. The purity of the initial components determines the composition of the deposited film. In the previous example, reactive sputtering of Al in nitrogen, water vapor or oxygen in the sputter gas can produce aluminium oxide along with AlN.

A very significant aspect of sputter deposition is the option to grow unusual phases or compositions that could not be grown in equilibrium processes at high temperature.

Because the plasma is "hot", reactions are fast and complete; rapid thermal quenching by condensation onto a (relatively) cold substrate preserves the composition achieved in the plasma. Phase segregation can be avoided as long as the films are not heated to the point where the different phases are free to form. Alternatively, sputtering onto a heated substrate can produce polycrystalline films and even epitaxy.

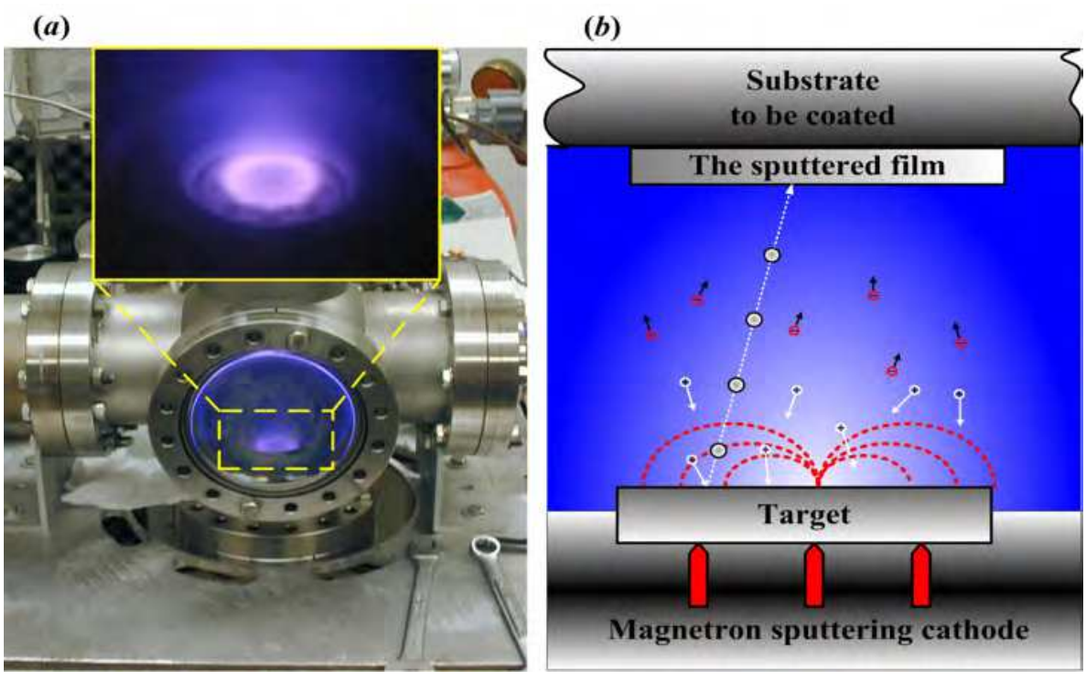

Fig. 2.1. RF magnetron sputtering system. a) actual system; b) schematic diagram. From (Ebdah 2011), used with permission.

Practical considerations can encourage the use of a particular target. Al sputtered in nitrogen is an ideal system. Only AlN forms from the reaction. The Al itself is inexpensive. Targets can even be made from industrial grade Al plate or bars (however, these materials usually contain small amounts of Cr, and chromium oxide CL is observed), making the use of multiple targets simple and convenient. In Kordesch's laboratory at Ohio University, multiple targets were fabricated from 2 inch diameter (50 mm) Al bars or from targets purchased from commercial vendors. Small plugs of the RE or transition metals were pressed into the aluminium targets. In this way, multiple dopants or multiple dopant percentages could be obtained with very simple methods. Zanatta used plates or chips of metal on the silicon target. For materials that do not melt, or alloy with the sputter target, this method could also be used.

Gallium was sputtered in our laboratory at Ohio University from a pressed powder target and also from a liquid metal target. In this case, the powder target was more difficult to use with regard to the dopant material, because there is no good mechanical contact between the powder and the metal insert. For the liquid target, some droplet ejection occurs during sputtering. The existence of metal droplets on the thin film surface is detrimental to device performance, especially if contact or insulating layers are deposited over the luminescent layer.

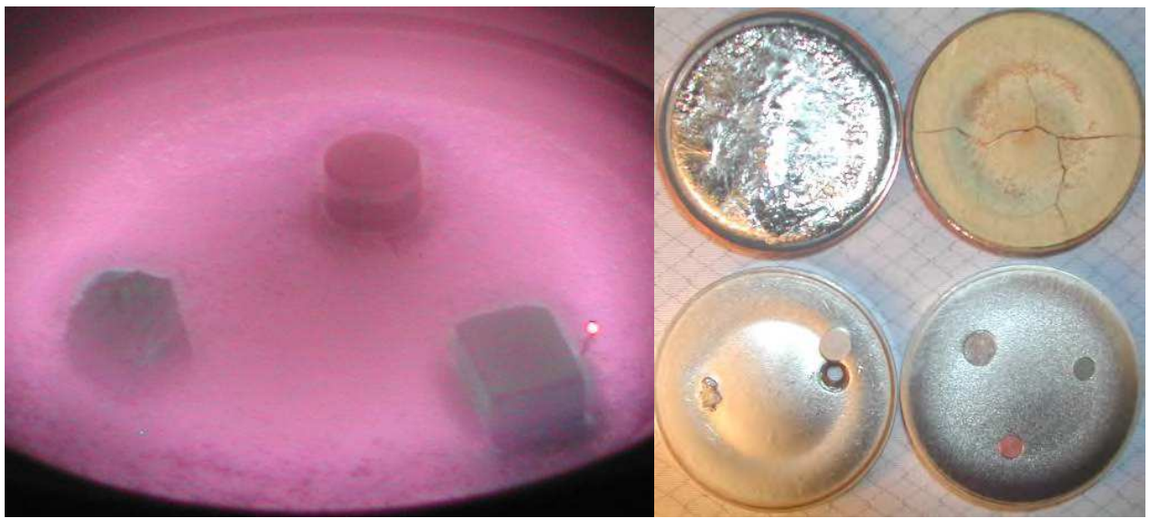

Fig. 2.2. Left: Target with (clockwise from top) Sm, Er, and Tb pieces during sputtering. Right: clockwise from top: Liquid metal Ga target in a copper cup, GaN powder target in a copper cup, aluminium target with Mn , Tb and Cu plugs, aluminium target with RE plug removed, and Tm dendrites pressed into the target. The circular depression in the targets at about ½ the radius is the "racetrack", where the plasma is confined by the magnets to improve the efficiency of the sputter process. All targets are 50 mm diameter.

In practice, the targets used were mostly 50 mm diameter, 6 mm thick disks of aluminium. The RE or transition metal plugs were obtained commercially as rods of 3 – 12 mm diameter. Plugs were cut from the rods and pressed into holes in the aluminium target. Manganese, for example, could only be purchased as a powder, so the powder was pressed into the 6 mm diameter hole. Some RE metals were obtained as dendrites or split fragments. These could be pressed into the softer aluminium target by force, even if voids were left around the RE material. Typical power levels were from 100-200 Watts RF (13.56 MHz) power at 2-10 mTorr pressures of nitrogen. This is the equivalent of 5-10 Watts/cm^2. The substrates could be heated from the back by using a quartz lamp with a parabolic reflector focussed onto the back of the substrate, or cooled by clamping the substrates to a copper cold finger cooled with dry ice. We have not used liquid nitrogen to cool the samples. First, the lower temperature will condense water onto the sample, and second, there are stresses that come from warming a film grown at low temperature to 300 K, just as there are stresses in films cooled from a high temperature deposition.

Aluminum, gallium, beryllium, scandium, boron, silicon, silicon nitride, aluminium oxide, zinc, hafnium, titanium and alloy targets were used. Dopant RE metals such as Er, Tb, Gd, Tm, Sm, Pr and Ho were used, as well as Cr, Cu, Mn, Mg, Si, C, Ti, Sn, Ag. The sputter target is always below the sample/substrate to avoid particulates formed in the sputter process from falling onto the substrate (see Fig. 2.1).

An important consideration for RE doping in the nitrides is the stability of the host material. Many RE nitrides decompose when in contact with water or humid air, which causes a reaction resulting in ammonia and a RE oxide. AlN, BN, GaN, SiN and ScN are not soluble in water. In our experiments, beryllium nitride was also stable in humid air. There is

considerable controversy over the role of oxygen in promoting the luminescence of RE ions in the nitrides. It is not known if the RE nitrides in a nitride host decompose or remain bonded to the N atom.

Finally, it should be pointed out that no electronic doping is observed in the amorphous nitride films. Partially, this is due to the fact that most of the amorphous nitride films are insulators, with the exception of n-type GaN. Electronic doping with Mg or Si was not successful, because the dopants react to form nitrides in the plasma, making the dopants commonly used in crystalline GaN for example, ineffective in amorphous nitrides.

2.2 Cathodoluminescence measurements

2.2.1 CL at room temperature and above

For CL measurements at 300 K and above, a simple system build in a six-way stainless steel cross with copper sealed flanges was used. The system was pumped with a 450 L/sec turbomolecular pump. A CRT electron gun with deflection plates was adapted to a multi-pin electrical feedthrough. The electron gun was powered with a laboratory-built power supply. The electron beam voltage could be varied up to 2.8 kV. Focus controls allowed the beam to be focussed onto the sample and to observe the spot on the sample through a vacuum viewport for optimization. The CL spot on the sample was then focussed onto the entrance slits of a monochromater using a lens.

The sample was illuminated with the electron beam from one side, the viewport was at 90 degrees from the electron gun. The sample was placed at 45 degrees to both arms of the cross. An aperture was placed in front of the sample between the sample and electron gun to block the visible light spot from the filament. The deflectors on the electron gun make it possible to steer the electron beam through the aperture while the direct light from the hot filament is blocked by the aperture.

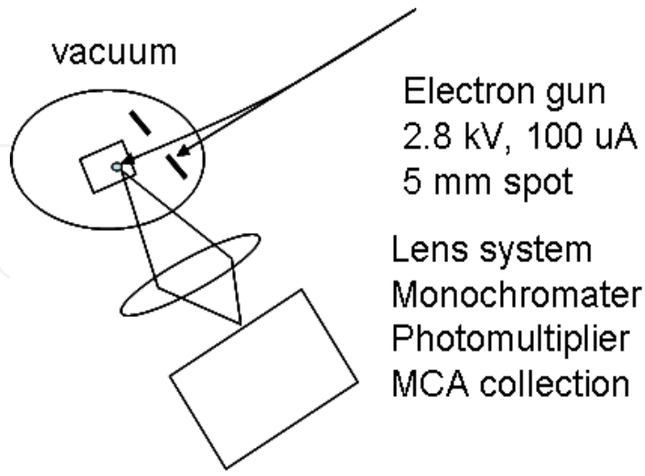

Fig. 2.3. Experimental setup for CL.

A commercial Luminoscope was also used for some CL measurements. The Luminoscope is meant to be used for geological specimens, and is equipped with a vacuum chamber that replaces the stage of a light-optical microscope. A window allows microscopic observation of

the sample surface during electron illumination. A gas discharge electron source is used to generate an electron beam of up to 30 kV. The Luminoscope can be used to take color micrographs of the sample surface. A drawback to spectroscopic measurements in the Luminoscope is the necessity to remove the gas discharge spectrum (He) from the CL spectra.

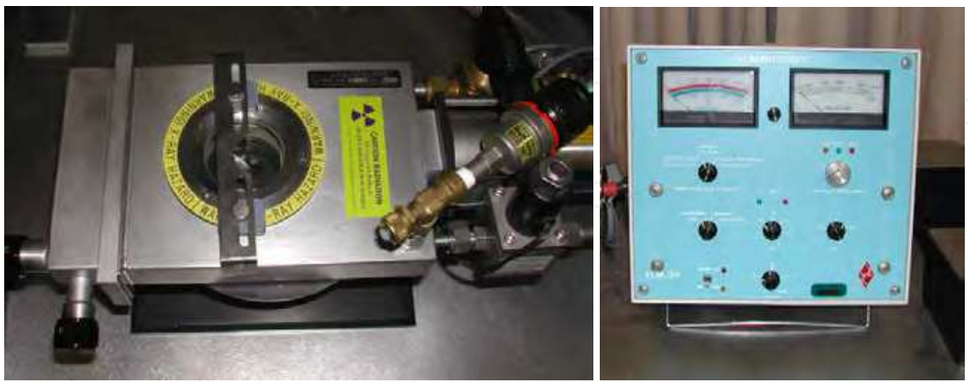

Fig. 2.4. Left: Lumiscope sample holder. Right: Lumiscope control and electronics.

2.2.2 CL at low temperature

Low temperature CL spectroscopic analysis was measured in our laboratory at cryogenic temperatures and excitation conditions using experimental setup shown in Fig.2.5. Typically samples were mounted on the cold finger of a closed-cycled helium refrigerator operating down to 6K. The CL was generated by the Staib Instruments, Inc. Electron Gun EK-20-R equipped with a beam blanker (repetition rate: DC to 1 MHz) electron gun system being in common vacuum (of 5×10^{-7} Torr) with the cryostat. The electron beam was incident upon the sample at a 45° angle from an electron gun. The CL depth of the excitation could be easily varied by varying the electron acceleration voltage between 500eV up to 20 keV.

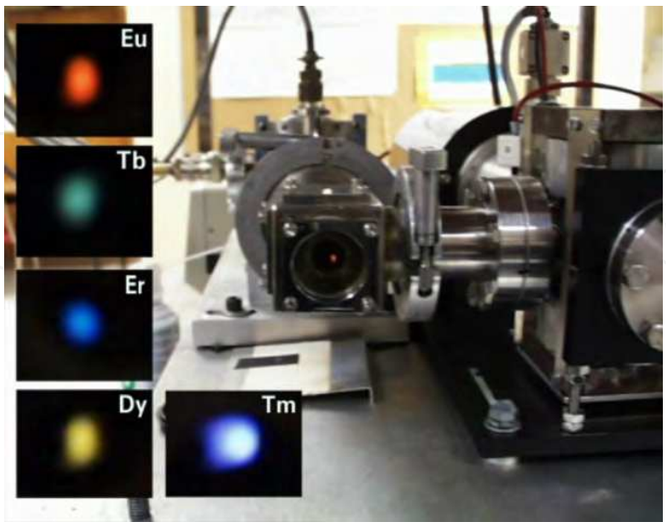

Fig. 2.5. Front view of a low temperature cathodoluminescence experimental setup operating between 6K- 330K and electron acceleration voltage up to 20 kV. Insets show color emissions from different RE-doped III-nitrides.

2.2.3 CL in the electron microscope

Cathodoluminescence attachments can be obtained for both scanning electron microscopes (SEM) and transmission electron microscopes (TEM). In the simplest SEM versions, a parabolic mirror is mechanically inserted into the specimen chamber above the sample, with a hole in the mirror for the passage of the electron beam. The light from the sample CL is reflected onto a photomultiplier tube and used to form a scanned image based on the CL yield. In advanced systems, and monochromater is added to the optical system so that spectroscopically resolved images can be generated. Similar systems are used in TEM, but without a CL image. Only spectroscopy is possible in the TEM. CL based images can be obtained in scanning TEM, STEM.

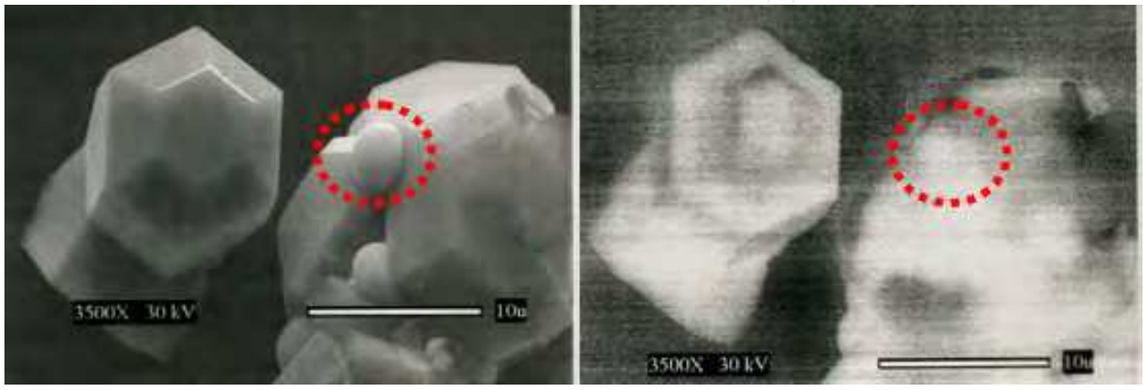

Fig. 2.6. Left: GaN crystallites in the SEM. A bit of a-GaN is shown in the stippled circle. Right: The same area, showing CL from the a-GaN and c-GaN. This image was one of the first experimental observations of a-GaN. (Hassan 1998).

3. Cathodoluminescence of rare earth doped amorphous nitrides

In the last two decades it has been shown that the incorporation of RE elements as dopant atoms into III-nitride semiconductors such as GaN, AlN and their alloys, both crystalline and amorphous, leads to a temperature-stable luminescence whose wavelength is nearly independent of the specific semiconductor host (O'Donnell 2010). Luminescence from these materials having amorphous morphology grown on variety of substrates, and doped by implantation or during the growth with Ce (Aldabergenova, Osvet et al. 2002) , Pr (Maqbool, Ahmad et al. 2007; Maqbool, Richardson et al. 2007; Maqbool and Ahmad 2009), Sm (Zanatta, Ribeiro et al. 2001; Weingartner, Erlenbach et al. 2006; Maqbool and Ali 2009), Eu (Aldabergenova, Osvet et al. 2002), (Weingartner, Erlenbach et al. 2006), (Caldwell, Van Patten et al. 2001), Gd (Maqbool, Ahmad et al. 2007),(Maqbool, Kordesch et al. 2009), Tb (Aldabergenova, Osvet et al. 2002), (Weingartner, Erlenbach et al. 2006),(Richardson, Van Patten et al. 2002), (Jadwisienczak, Lozykowski et al. 2000), Dy (Weingartner, Erlenbach et al. 2006), Ho (Maqbool, Ali et al.; Aldabergenova, Frank et al. 2006; Maqbool, Kordesch et al. 2009), Er (Gurumurugan, Chen et al. 1999; Chen, Gurumurugan et al. 2000; Dimitrova, Van Patten et al. 2000; Dimitrova, Van Patten et al. 2001; Zanatta, Ribeiro et al. 2005), Tm (Maqbool, Kordesch et al. 2009) and Yb (Weingartner, Erlenbach et al. 2006) has been reported so far. In particular, RE doped GaN-nitrides based electroluminescent devices (ELDs) have been shown to have a versatile approach for the fabrication of variety of electrically driven optical light

sources with narrow line-width emissions from the ultraviolet to the infrared (Steckl 1999). Thus optoelectronic devices utilizing $4f^n$ transitions appearing in the nitrides forbidden band gap "window" are practically viable with these semiconductors (O'Donnell 2010). Recently it was demonstrated that the low voltage-operation of current-injected red emission from a crystalline *p*-type/Eu-doped/*n*-type GaN epilayers light emission diode operating at room temperature (Nishikawa, Kawasaki et al. 2009; Kasai, Nishikawa et al. 2010; Nishikawa, Furukawa 2010; Dierolf 2011) together with demonstrations of stimulated emission from Eu^{3+} doped GaN and AlGaN layers on a Si substrate proved in principal that optoelectronic devices covering the UV, visible and IR regions might be fabricated (Park and Steckl 2004; Park and Steckl 2005; Park and Steckl 2006).

These new results suggest a novel way to realize III-nitride semiconductors-based red emitting, current driven light emitting devices, as well as other primary colors and their mixture, monolithic devices. In the past the feasibility of using the RE-doped amorphous III-nitrides (a-III-nitrides) for light emitting applications was also demonstrated (Dimitrova, Van Patten et al. 2000; Dimitrova, Van Patten et al. 2001; Richardson, Van Patten et al. 2002; Maqbool, Kordesch et al. 2009), (Kim, Shepherd et al. 2003; Kim and Holloway 2004). However, to make these devices commercially viable, the internal quantum efficiency of the active RE-doped layers has to be significantly improved. The future success of the RE-doped III-nitrides optoelectronics, both crystalline and amorphous based will most probably depend on engineering of multilayer structures. In these devices an enhancement of RE^{3+} ion luminescence intensity can be achieved through *e.g.* (a) modification of the RE^{3+} center environment and (b) localization of carriers in the vicinity of emitting RE^{3+} ion center. The former one can be achieved through engineering stress/strain parameters during the growth process, whereas the last one will results from carriers confinement in the quantum structures.

In general, the majority available research papers focus on RE-doped crystalline III-nitride semiconductors with less emphasis on a-III-nitrides used as hosts for optically, electrically and/or magnetically active RE dopants. The amorphous semiconductors including a-III-nitrides as hosts for RE doping have many of the desirable qualities of the crystalline materials; however they also offer unique features rooted in the nature of the amorphous matrix (Adachi 1999; Singh 2003; Street 2010). The most important are that a-III-nitrides can be achieved at higher growth rates and lower temperatures, substrate selection and resulting lattice mismatch is not a significant obstacle here, they do not easily recrystallize when subjected to thermal processing and that they can adapt the RE ions in concentrations far beyond those given by the solubility limit found in their crystalline counterparts. Furthermore, it is known that a-III-nitrides show a natural tendency to develop a state free gap [(Chen and Drabold 2002; Drabold 2010). Also a-III-nitrides, unlike other amorphous systems or glasses which look locally very similar to the crystal, apparently have local environments very different from the main crystalline morphology what make them potentially useful as hosts for optically and electrically active RE dopants. It was demonstrated that the RE ions luminescence intensity, when intended for optoelectronic applications, can be increased by proper structural tailoring of a-III-nitride matrices. At the same time the RE^{3+} ion excitation and de-excitation processes are more dependent on the local RE ion environment than in crystalline semiconductors due to the lack of long range ordering in amorphous host (Zanatta, Ribeiro et al. 2006). The *f-f* transitions are forbidden, but they are partially allowed when the wave functions are mixed with those of opposing parity. This always occurs on localized ions in non-central symmetrical lattices. The

forbidden nature of these transitions results in long radiative lifetimes when the selection rules are relaxed. Placing trivalent rare earth ions in amorphous solids can still result in characteristic emission from these intra-4*f* transitions despite the lack of a crystalline host structure (O'Donnell 2010). In both cases RE luminescence depends very little on the nature of the host and the ambient temperature. The 4*f* orbitals of RE ions incorporated into semiconductors, including a-III-nitrides, are so deeply buried within the electronic shell that the energy levels of the $4f^n$ configuration are only slightly perturbed compared to free ion energy levels indicating large independence from the chemical surrounding and thus the choice of the host material (Wybourne and Smentek 2007). RE ions when doped to a-III-nitrides are known to exhibit sharp and well-defined luminescence which arises mostly from internal transitions between 4*f* levels within RE^{3+} ion. Because of the shield provided by the outer $5s^2$ and $5p^6$ shells, the wavelength involved in these intra-4*f* transitions is less temperature sensitive and rather weakly depends on the a-III-nitride host. On the other hand the mechanism behind the activation of RE are known to be sensitive to a local host details such as atomic structure and optical band gap which defines which RE transitions can be excited.

3.1 Rare earth doping

Doping of a-III-nitrides is generally achieved *in situ* ; however it can be also done by RE ions implantation (Aldabergenova, Frank et al. 2006). In the former case doping typically takes place during sputtering process in which RE-doped a-III-nitride is formed from Ga, Al and RE atoms removed from metal targets by momentum transfer from an RF plasma. The sputtering growth of a-III-nitrides is explored much less than other technologically important amorphous semiconductors e.g a-Si doped with RE impurities (Iacona, Franzo et al. 2009). Ion implantation has been used extensively to *ex situ* dope III-nitride crystalline semiconductors with variety of rare earth ions. Excellent review concerning this issue is available (O'Donnell 2010). There are a limited number of papers on RE ions implantation to a-III-nitrides and resulting luminescence spectra (Jadwisienczak, Lozykowski et al. 2000). Ion implantation is a well established technique, which provides good control of the concentration profile in the sample. However, because of the unavoidable damage associated with the implantation process, typically a high temperature annealing step is imperative. This is due to the fact that when heavy atoms like RE metals are implanted to an amorphous semiconductor they can introduce both a chemical change in the substrate, in that they can introduce a different element than the host or induce a nuclear transmutation, and a structural change, in that the morphology of the host can be damaged or even destroyed by the energetic collision cascades induced by implanted heavy RE ions (Kucheyev, Williams et al. 2004).

It is known that the thermal anneal of the a-AlN films affects not only the luminescent properties of the films, but also their optical band gap and chemical characteristics. As a result of thermal treatments of RE-doped a-III-nitrides at increasing temperatures the optical-absorption edge of amorphous films may change indicating the Al and N bonding environment modification (Zanatta, Ribeiro et al. 2005). Based on the available experimental results it is clear that RE-doped a-III-nitrides subjected to isochronal thermal annealing treatments indeed most likely underwent partial removal of both structural and chemical disorder resulting in modification of RE ions local environments as it is shown in Figs. 3.1 and 3.2 for Er-doped a-AlN films (Gurumurugan, Chen et al. 1999; Jadwisienczak, Lozykowski et al. 2000; Weingartner, Erlenbach et al. 2006).

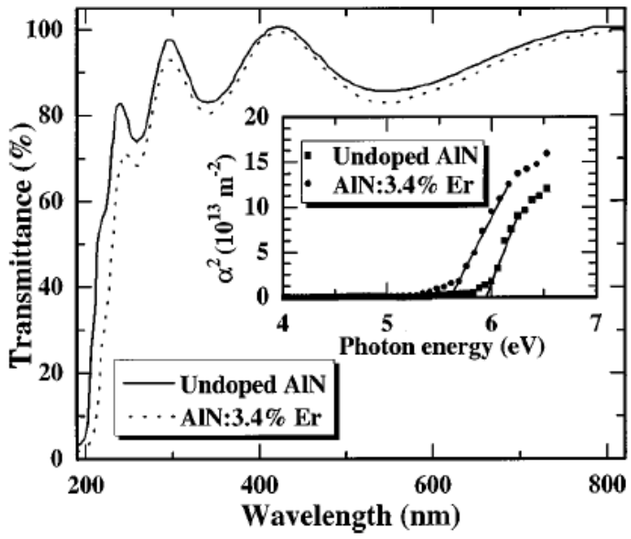

Fig. 3.1. Optical transmission spectra of undoped and Er-doped a-AlN thin films. Inset shows the photon energy dependence of the square of the absorption coefficient for undoped and Er-doped a-AlN thin films. After Ref. (Gurumurugan, Chen et al. 1999)

It is documented in the literature that thermally annealed amorphous semiconductors experience some structural reordering (not necessarily crystallization) (Gurumurugan, Chen et al. 1999). Figure 3.2 shows evolution of cathodoluminescence (CL) spectra of Tb-doped a-AlN films subjected to thermal annealing in nitrogen ambient up to 1100 ^{o}C.

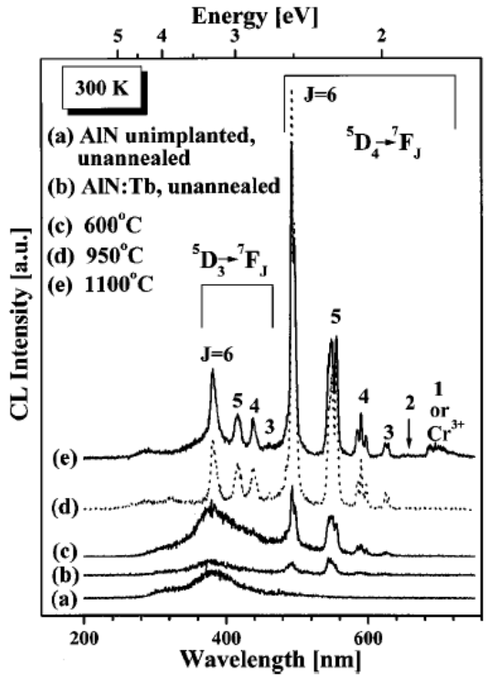

Fig. 3.2. Evolution of CL spectra in Tb-doped a-AlN films as a function of annealing temperature. After Ref. (Gurumurugan, Chen et al. 1999).

It is believed that when this takes place the dangling or broken bonds and/or the atomic rearrangements of the amorphous material may have great influence on the electronic states of amorphous host. The available reports show that the conducted x-ray diffraction analysis of as-grown or thermally treated RE-doped a-III-nitride thin films has not revealed any microscopic morphology changes in studied materials (see Fig. 3.3).

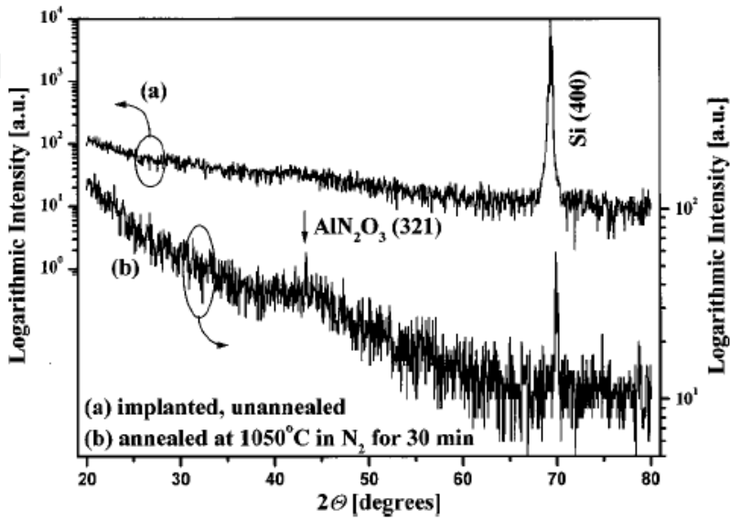

Fig. 3.3. XRD spectra of a-AlN thin films doped with Tb^{3+} ions. (a) unannealed and (b) annealed for 30 min at 1050 °C in nitrogen. Ref. (Jadwisienczak, Lozykowski et al. 2000).

As reported by Zanatta et al. (Zanatta, Khan et al. 2007) a-SiN doped with Sm and Tb exhibit significant enhancements of 4*f*-shell radiative recombinations upon thermal annealing due to a decrease in the density of deep and/or tail defects (suppression of the nonradiative processes). A similar observation was made for a-AlN:Ho system (Aldabergenova, Frank et al. 2006). Furthermore, in that study, the growth of small crystallites in initially mostly a-AlN:Ho host was observed after annealing above 900 °C. See Fig 3.4.

In order to avoid the implantation induced amorphous material morphological changes and defects due to ion implantation, simultaneous co-deposition of different RE metals during RF sputtering growth was demonstrated (Maqbool, Kordesch et al. 2009). This approach is an extension of a typical a-III-nitrides RF sputtering growth technique where RE ions concentration in resulting film is controlled by sputtering metals to target surface ratio. It is possible using this procedure to control the RE concentration in the sample over a wide range. Furthermore, this technique gave an opportunity to derive mixed RE-doped a-III-nitride systems where more complex interaction schemes defining energy transfer processes can be studied. However, there exist only limited papers reporting on this issue up to date (Maqbool, Kordesch et al. 2009). The single RE ion and multiple RE ions doping to a-III-nitrides should have typical doping effects in these hosts in the sense of controlling the electronic properties of the material and determining the Fermi level position. In contrast to unhydrogenated a-Si and hydrogenated a-Si:H where it was proposed that several different REs turned out to act as acceptors or donors (Tessler 1999) no similar postulate was considered in the case of RE-doped a-III-nitrides to date. It is uncertain at present if other than trivalent RE ions in a-III-nitrides can exist; however such a scenario is feasible

especially if one considers a plethora of possible RE ions configurations in amorphous matrix as well as the fact that RE ions are strong oxygen and other impurities getters. Systematic RE ion doping studies with controlled co-dopant concentrations are needed to validate this consideration in the future.

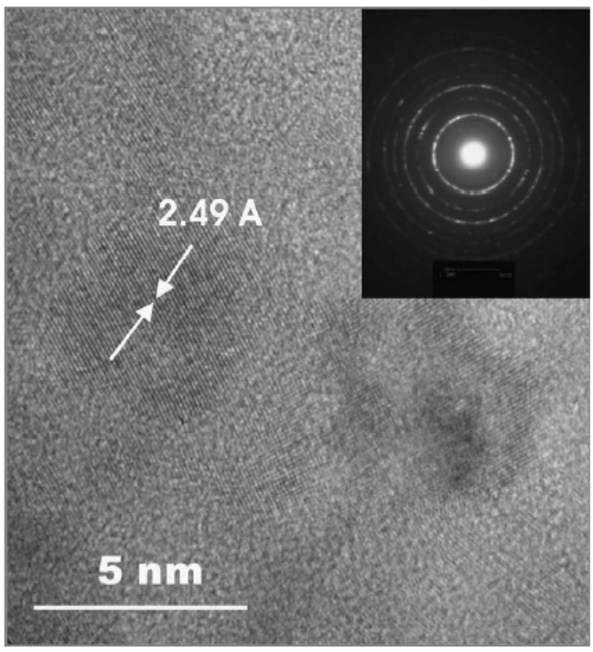

Fig. 3.4. High resolution micrograph showing small AlN crystallites embedded in as grown a-AlN film. The insert shows the pertaining diffraction pattern. After (Aldabergenova, Frank et al. 2006).

3.1.1 Rare earth excitation

The excitation processes of RE ions in a-III-nitrides, similarly to crystalline hosts, can be generally divided into two categories: direct and indirect excitation processes (Jadwisienczak, Lozykowski et al. 2000; Lozykowski, Jadwisienczak et al. 2000). The direct excitation process occurs in selective excitation of $4f^n$ electrons by photons (photoluminescence, PL) selective excitation or in cathodoluminescence (CL) and electroluminescence (EL) by collision with hot electrons. The indirect excitation process occurs via transfer of energy to the $4f^n$ electron system from electron–hole pairs generated by photons with higher energy than the band gap (PL excited above band gap), injected in forward bias *p-n* junctions, or generated by hot carriers in CL and EL. An excitation mechanism in CL and EL involves direct impact excitation of RE^{3+} ions by hot electrons, as well as an energy transfer from the generated electron–hole pairs or by impact excitation (or ionization) involving impurity states outside the 4*f* shell, with subsequent energy transfer to this shell. The most important, from an applications point of view, is the excitation of the RE ions by energy transfer processes from electron-hole (e-h) pairs or excitons. This process most probably involves the rare earth ion isovalent traps (Lozykowski, Jadwisienczak et al. 2000). Since there is no charge involved, the isoelectronic center forms the bound states by short range central cell potential. After an isoelectronic trap has captured an electron or a

hole, the isoelectronic trap is negatively or positively charged, and by Coulomb interaction it will capture a carrier of the opposite charge creating a bound exciton. There are three possible mechanisms of energy transfer (Lozykowski 1993). The first is the energy transfer process from excitons bound to structured isoelectronic centers to the core electrons. This takes place as a result of the electrostatic perturbation between the core electrons of the RE structured impurity and the exciton, effective-mass-like particles. The second mechanism is the transfer of energy to the core electrons involving the structured isoelectronic trap occupied by electron (hole) and free holes (electrons) in the valence (conduction) band. The third mechanism is the transfer through an inelastic scattering process in which the energy of a free exciton near a RE structured trap is given to the localized core excited states. If the initial and final states are not resonant, the energy mismatch must be distributed in some way, e.g., by phonon emission or absorption. If the atomic core excitations are strongly coupled to the host phonons, the energy transfer probability is likely to be higher (Lozykowski 1993). Strong phonon coupling may also be desirable in ensuring that relaxation down the ladder of the core excited state occurs quickly, thus preventing back transfer. However, for efficient radiative recombination, the phonon coupling should not be strong, in order to prevent core de-excitation by nonradiative multiphonon process. It is natural to assume that when isoelectronic impurity atoms, in this case RE ions, are incorporated in a-III-nitride host, they modify local vibrational properties in a definite way. Thus, there should be observed distinct vibrational frequencies associated with localized motion of the RE impurity in addition to the host lattice vibrations. In III-nitrides the threshold energy for electron damage in amorphous films is considerably smaller contrary to crystalline compounds (Zanatta, Ribeiro et al. 2005). Moreover, energetic electron irradiation may create defects that are not possible with photons with energies in the visible energy range. These additional defects, mainly broken bonds and atomic displacements, act as nonradiative centers that considerably reduce the luminescence efficiency of a-III-nitride semiconductor. On the other hand, RE ions are high efficiency recombination centers that effectively compete with other non-radiative processes taking place in a semiconductor host. As a result, when irradiating the RE-doped a-III-nitrides with up to a few keV energy electrons, most of the electron-hole pairs recombine preferentially through the RE ions. Luminescence after photon excitation, on the other hand, behaves in a different manner and is very strongly excitation wavelengths dependent (Gurumurugan, Chen et al. 1999; Jadwisienczak, Lozykowski et al. 2000; Zanatta, Ribeiro et al. 2005).

In photoluminescence each absorbed photon with energy higher than the band gap produces a single electron-hole pair while in cathodoluminescence, high energy single electrons generate a huge number of ''hot'' e–h pairs, reducing the energy from tens of keV to zero (Jadwisienczak, Lozykowski et al. 2000). In general, the optical excitation process demands that the *4f* electrons are excited absorbing energy. In a-III-nitride materials with large band gap like a-GaN and a-AlN this can occur with a direct absorption to one of the transitions of upper energy of the RE^{3+} ion degenerated with the conduction band or via transfer of energy from a defect related Auger resonant process between the RE^{3+} ion states and the dipole formed by the *s*-like conduction band states and *p*-like dangling bond states. The PL of RE^{3+} ion in a-III-nitrides is obtained by an indirect excitation process via transfer of energy to the $4f^n$ electron system from e-h pairs. In electron beam excitation (CL), however, the RE^{3+} ions are excited by direct impact with hot electrons, as well as by energy transfer processes from the generated e–h pairs or by impact excitation (or ionization)

involving other impurities (or complex defects) with subsequent energy transfer to the RE 4*f*-shell electrons. Generally the excitation by energetic electrons produces emission via all possible luminescence mechanisms available in a semiconductor. Another factor which may play a role in excitation and emission processes is the charged nature of excitation: uncharged photons in PL versus negatively charged electrons in CL. The excitation depth in PL and CL are also different due to the strong absorption of the excitation photons in a-III-nitrides within a few tens of nanometers layer; whereas the electron penetration depth is electron acceleration energy dependent and can reach up to a few hundreds nanometers (Jadwisienczak, Lozykowski et al. 2000). Figure 3.5 and Fig. 3.6 show examples of CL spectra of the rare earth (Tm, Tb, Dy, Sm, Eu, Er and Yb) doped a-AlN layers [(Gurumurugan, Chen et al. 1999; Jadwisienczak, Lozykowski et al. 2000; Weingartner, Erlenbach et al. 2006). The transitions corresponding to the strongest emission lines are indicated by their energy level assignments. It was reported in these studies that all RE-doped a-AlN layers show (even untreated) pronounced RE^{3+} ion optical spectra at room temperature.

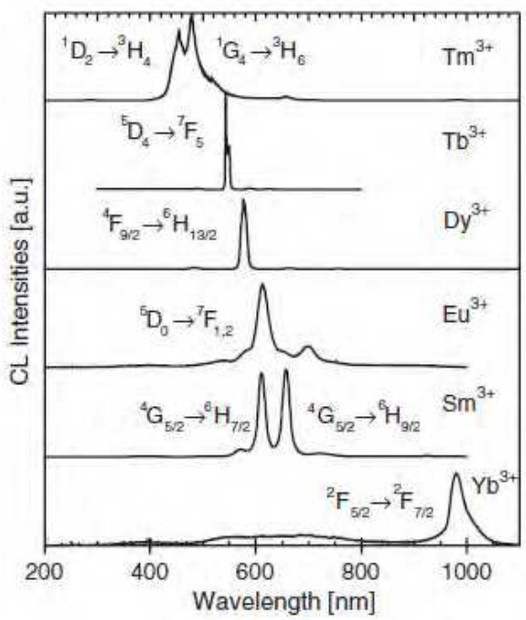

Fig. 3.5. Survey of CL spectra of RE-doped a-AlN thin films. After Ref. (Weingartner, Erlenbach et al. 2006).

The RE ion excitation process responsible for observed EL from RE-doped a-III-nitrides is very similar to described above CL. Thus CL and EL spectra, in general, shows similar spectra features. It was reported that in cases of the Er and Tb-doped a-AlN alternating-current thin-film electroluminescent devices the EL and CL spectra are very similar (Dimitrova, Van Patten et al. 2000; Dimitrova, Van Patten et al. 2001; Richardson, Van Patten et al. 2002).

Typical transient analysis of luminescence observed from RE-doped III-nitride crystalline semiconductors stimulated by different means provided detailed insight into energy migration and excitation processes observed in these technologically important materials. There are a very limited number of papers reporting on luminescence (CL, EL) kinetics of RE-doped a-III-nitride up to date (Richardson, Van Patten et al. 2002). It is known that the nonradiative decays of

excited RE ions in semiconductors, including RE-doped a-III-nitrides, are phonon dependent (Jadwisienczak, Lozykowski et al. 2000). Furthermore, at sufficiently high concentrations of RE ions, nonradiative decay can occur via ion pair cross-relaxation or energy migration and finally transfer to quenching centers (Jadwisienczak, Lozykowski et al. 2000). For low RE concentration, where ion–ion pair relaxation or energy migration and transfer to quenching centers has low probability, excited RE electronic states gave up energy radiatively by purely electronic or phonon assisted transitions or nonradiatively by the emission of a single phonon or multiphonon. Nonradiative relaxation between RE^{3+} ion *J*-manifolds in solid state host, including reported CL kinetics of Tb-doped a-AlN , typically requires the participation of several phonons and occurs at slow rates, while relaxation between crystal field levels of a *J*-manifold by single or two phonon processes is much faster. It is known that the rate of multiphonon emission is strongly dependent upon the number of phonons required to conserve energy, and hence on the size of the energy gap to the next lowest energy level. The detailed investigations of nonradiative decay of RE ions in a-III-nitrides have not been done yet; however it is expected that that multiphonon transitions involving the emission of a maximum of a few phonons will effectively compete with radiative transitions. Furthermore, it is expected that the temperature dependence of the decay rates will show that relaxation occurs mainly by high energy phonons. It is worth noting that energy separation of *J*-crystal field levels shows only small changes with the host (Jadwisienczak, Lozykowski et al. 2000; Jadwisienczak, Lozykowski et al. 2000). Differences in the rate of nonradiative decay from a particular RE energy level arise from the phonon energy spectrum of the host material and the strength of the RE ion–lattice coupling. Local vibrational modes related to RE ions, their complexes, or others impurities present in a-III-nitride host will also play an important role in the above-discussed process; however these assumptions will have to be critically confirmed in the future.

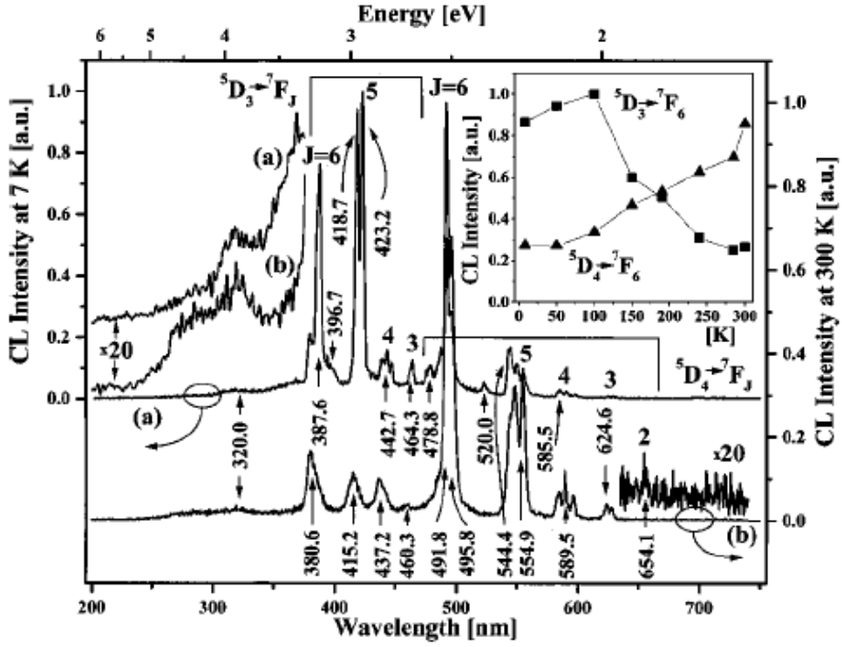

Fig. 3.6. CL spectra of a-AlN:Tb recorded at cryogenic and room temperature. The inserts show the total integral intensity of the dominant 4*f*-shell transition lines as a function of temperature. After Ref. [(Jadwisienczak, Lozykowski et al. 2000)].

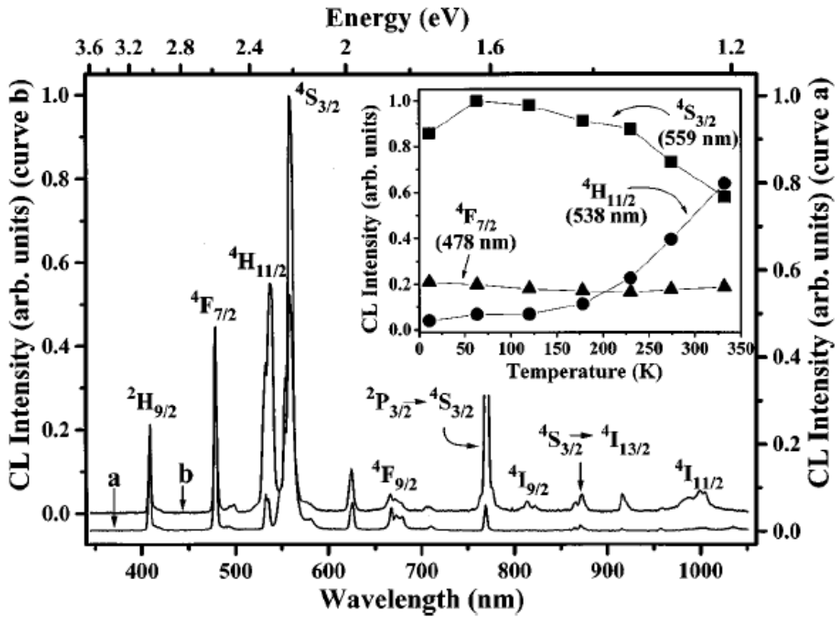

Fig. 3.7. CL spectra of a-AlN:Er recorded at cryogenic and room temperature. The inserts show the total integral intensity of the dominant 4*f*-shell transition lines as a function of temperature. After Ref. [(Gurumurugan, Chen et al. 1999)].

The local environment of the RE^{3+} ions, and consequent luminescence intensity, in a-III-nitrides can be greatly influenced by the presence of nitrogen atoms, intrinsic impurities, larger clusters and thermal treatments stimulating morphological changes at micro-scale. This in turn affects the optical activity of RE^{3+} ion by enhancing or quenching luminescence originating from 4*f*-shalls transitions. The vulnerability of amorphous semiconductors to defects generation in CL and EL is rather straight forward considering the threshold energy for electron damage in amorphous networks being much smaller (1 keV) comparing to crystalline semiconductors (100 keV) (Zanatta, Ribeiro et al. 2005). This fact creates an interesting research opportunity for RE-doped a-III-nitrides in the search for more effective energy transfer process between RE ions and amorphous host. It is known that the III-nitride quantum structures with dimensions close to the excitonic Bohr radius exhibit electronic and optical properties affected by the confinement of electrons in one, two, or three dimensions (Ihn 2010). The principal consequences of quantum confinement are an increase in the band gap energy and increased probability of radiative transitions. Confinement of carriers in real space causes their wavefunctions to spread out in momentum space, increasing the probability of radiative processes due to greater wavefunction overlap. Because of the modification of their band structure, doping such confined systems with RE^{3+} ions can also help to overcome some of the nonradiative de-excitation problems associated with RE-doped III-nitride. Quantum confinement affects also carrier lifetimes and their degree of localization in real space. This in turn modifies the Auger back-transfer processes that limit luminescence efficiency and increases the interaction probability between the confined carriers and the RE^{3+} ions. In general, the RE^{3+} ion radiative quantum efficiency strongly depends on the carrier mediated energy transfer processes, which have to compete with nonradiative recombination channels abundant in a-III-nitrides. It is known that RE^{3+} ions induce significant local site distortion

due to their large radii as well as gettering effect (O'Donnell 2010). It was theoretically shown that the Coulomb excitation of 4*f* electrons near interface of heterostructures, where certain degree of disorder is expected, is more effective than a similar excitation in the bulk semiconductors (Zegrya and Masterov 1995; Zegrya and Masterov 1996; Zegrya and Masterov 1998; Masterov and Gerchikov 1999). Also, as discussed above, the thermal annealing process of RE-doped a-III-nitride changes grain boundary, where RE ions most probably reside, resulting in change of RE ion local environments and their optical activities due to relaxed 4*f*-shell electron-lattice coupling. In that sense one may assume that RE^{3+} ions located at the surface of the a-III-nitride nano-grains may act as grain boundary activators. It has now been well established that semiconductor nano-clusters can act as efficient luminescence sensitizers for RE ions in wide band gap solid states (Iacona, Franzo et al. 2009). Moreover, it appears that it is not necessary for the semiconductor inclusions to be crystalline – amorphous nano-clusters are at least as efficient as nano-crystals (Kenyon and Lucarz). The customary observation is that absorption of photons by semiconductor nano-clusters results in excitation of RE ions via an efficient transfer mechanism to unexcited RE ions. Such a process is significant for two reasons: firstly, the effective absorption cross-section of the RE ion is increased by several orders of magnitude (Kenyon, Lucarz; Kik 2003), and secondly, it becomes possible to excite the RE ions via the broad-band absorption of the semiconductor nano-clusters (Kenyon, Chryssou et al. 2002; Kik 2003; Iacona, Franzo et al. 2009). Moreover, the prospect of engaging amorphous nano-clusters to activate RE ions in a-III-nitrides removes the prerequisite to control tightly the crystallinity and size distribution of nano-cluster sensitizers thus greatly simplifying material processing. More studies are necessary to clear this point. It is our belief that the quenching mechanism should not depend on the form of sample preparation rather than on the final RE ion local symmetry inducing site degeneracy required for observing peculiar intra 4*f*-shell transitions.

3.2 Amorphous nitrides: Examples

Most of the metal nitrides are $M^{3+}N^{3-}$ compounds, so that no special considerations are necessary for RE emission. There is still some controversy about the site of the RE ion in crystalline nitrides. In an amorphous solid, bonding to the N as a (3+) ion is the most obvious choice. However, it is the case that sharp lines are observed from RE ions in the amorphous hosts, and in some cases the analogue of "crystal field splitting". There are probably several types of sites for the RE ion, but not enough to broaden the emission peaks excessively.

Because the emission lines in RE ions are well known, in most cases the experimental task is to see which transitions are observed in each host. Post growth heat treatment of the as-gown nitrides often improves the intensity of the RE emission in the nitrides. Because there is no "annealing" in the sense of crystal structure or long range lattice improvement, the heating process can cause the removal or transport of materials unrelated to the nitride structure. There could be removal of hydrogen, for example, or diffusion of oxygen. The reaction of water trapped in the film due to background gasses in the vacuum or in the heat treatment gas during post growth thermal treatment would include the removal of N atoms as ammonia, affecting the basic M-N bonds. Some rearrangement of the short range nitride structure is possible.

Even though there can be much larger RE concentrations in sputter deposited nitride films compared to ion implanted films, there is no dramatic increase in intensity with higher RE concentrations. It must be assumed that a large number of the RE ions are not optically active in the as-grown amorphous films. Heat treatment or oxygen additions increase the number of active RE ions. Co-doping with other (3+) ions sometimes also improves the emission intensity of RE ion luminescence. One of the possibilities is that the (3+) impurity occupies the inactive sites and displaces the RE ions onto active sites. Optical interactions are also possible.

3.2.1 Amorphous silicon nitride

The bulk of studies on amorphous silicon nitride doped with RE ions are due to Zanata and co-workers. Silicon is multivalent, so that a-SiN may well result in a RE^{3+} ion without any further need for charge compensation.

3.2.1.1 Erbium, Holmium, Dysprosium Samarium and Praseodymium

Zanatta and co-workers studied Pr, Sm, Dy, Ho, and Er in amorphous SiN films.

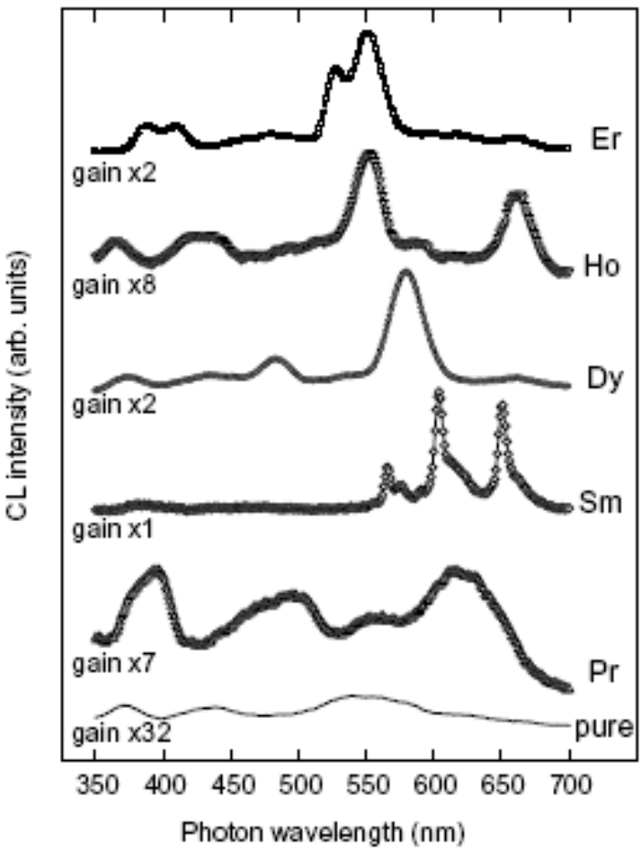

Fig. 3.8. Cathodoluminescence spectra of RE^{3+}-doped a-SiN films deposited by co-sputtering. The spectra have been acquired at room temperature by using 15 keV electrons and a current density of 10 nA. All spectra were normalized and vertically shifted for comparison. From (Zanatta, Ribeiro et al. 2004).

The CL spectra of the present RE-doped a-SiN films are shown in Fig. 3.8. In addition to the levels close to 490 nm these new transitions correspond to Er^{3+} ions ($^4G_{11/2}$ to $^4I_{15/2}$ at 390 nm, $^2H_{9/2}$ to $^4I_{15/2}$ at 410 nm); Ho^{3+} ions ($^5G_5$ to $^5I_5$ at 430 nm, $^3H_5$ to $^5I_5$ at 360 nm); Sm^{3+} ($^4K_{11/2}$ to $^6H_{5/2}$ at 380 nm); and Pr^{3+} ions ($^1S_0$ to $^1D_2$ at 370 nm, $^1S_0$ to $^1I_6$ or $^3P_1$ at 395 nm). The variations observed in the luminescence intensity probably occur because of differences in the RE content; Er (0.5 at.%), Ho (0.3 at.%), Dy (0.3 at.%), Sm (0.5 at.%), and Pr (0.2 at.%). (Zanatta, Ribeiro et al. 2004)

3.2.1.2 Samarium and terbium

Most of the luminescence features present in the 400–850 nm wavelength range (Fig. 3.9) correspond to optical transitions due to the Sm^{3+} and Tb^{3+} ions (Dieke 1968): Sm1 at ~565 nm ($^4G_{5/2} \rightarrow {}^6H_{5/2}$), Sm2 at ~605 nm ($^4G_{5/2} \rightarrow {}^6H_{7/2}$), Sm3 at ~650 nm ($^4G_{5/2} \rightarrow {}^6H_{9/2}$), Tb1 at ~485 nm ($^5D_4 \rightarrow {}^7F_6$), Tb2 at ~545 nm ($^5D_4 \rightarrow {}^7F_5$), Tb3 at ~590 nm ($^5D_4 \rightarrow {}^7F_4$), and Tb4 at ~625 nm ($^5D_4 \rightarrow {}^7F_3$). In addition to these, we also observe the Sm4 light emission at ~725 nm ($^4G_{5/2} \rightarrow {}^6H_{11/2}$), which is associated with the superposition of the $^4G_{5/2} \rightarrow {}^6H_{11/2}$ transition due to Sm^{3+} ions and the $^5D_0 \rightarrow {}^7F_0$, $^5D_0 \rightarrow {}^7F_1$, and $^5D_0 \rightarrow {}^7F_2$ transitions of Sm^{2+} ions. The infrared contribution Sm5 at ~810 nm corresponds to the $^5D_0 \rightarrow {}^7F_4$ transition and is exclusively due to Sm^{2+} ions (Dieke 1968).

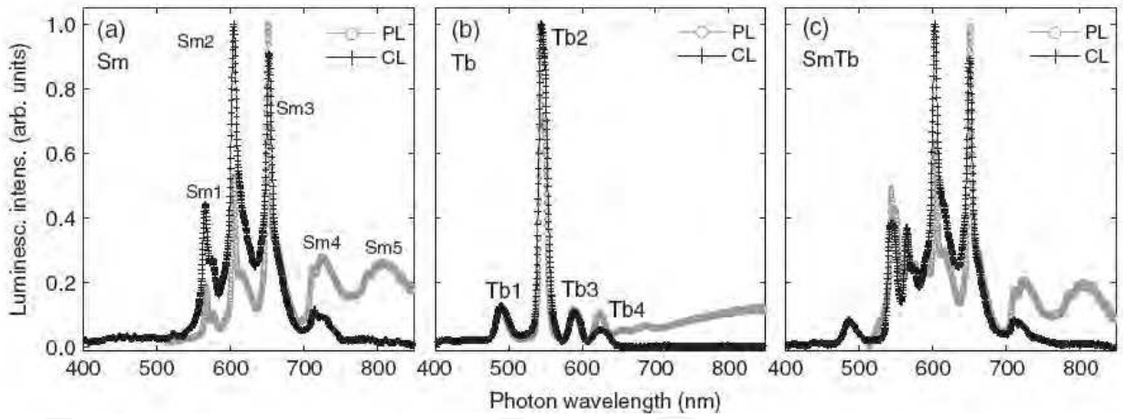

Fig. 3.9. Smarium and Terbium CL in amorphous silicon nitride. From (Zanatta, Khan et al. 2007).

3.2.2 Amorphous aluminum nitride

3.2.2.1 Erbium and terbium

The first RE spectrum in amorphous Aluminum Nitride (a-AlN) was that of Gurumurugan et al. (Gurumurugan, Chen et al. 1999). The spectra are shown in Figures and 3.7 (Jadwisienczak, Lozykowski et al. 2000).

3.2.2.2 Europium

Europium doped a-AlN was studied by Caldwell et al. (Caldwell, Van Patten et al. 2001).

The most significant result of this study was that thermal activation of the RE ion in a-AlN, which was found generally to increase the luminescence yield by a factor of up to 100, could

be matched or exceeded by the addition of oxygen during the growth of the film by sputtering. The luminescence yield increased over 600 times with the addition of oxygen to the sputter gas.

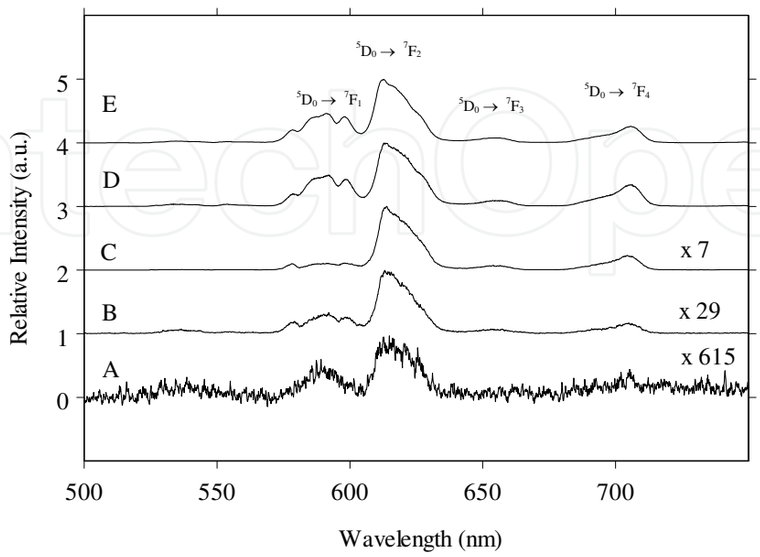

Fig. 3.10. CL spectra of a-AlN:Eu processed as follows: a) no oxygen, and no heat treatment, b) no oxygen, heated to 923 K. c) grown with 1.6% oxygen in nitrogen, d) grown in 3.8% oxygen in nitrogen, e) grown in 20% oxygen, with the balance nitrogen. From (Caldwell, Van Patten et al. 2001).

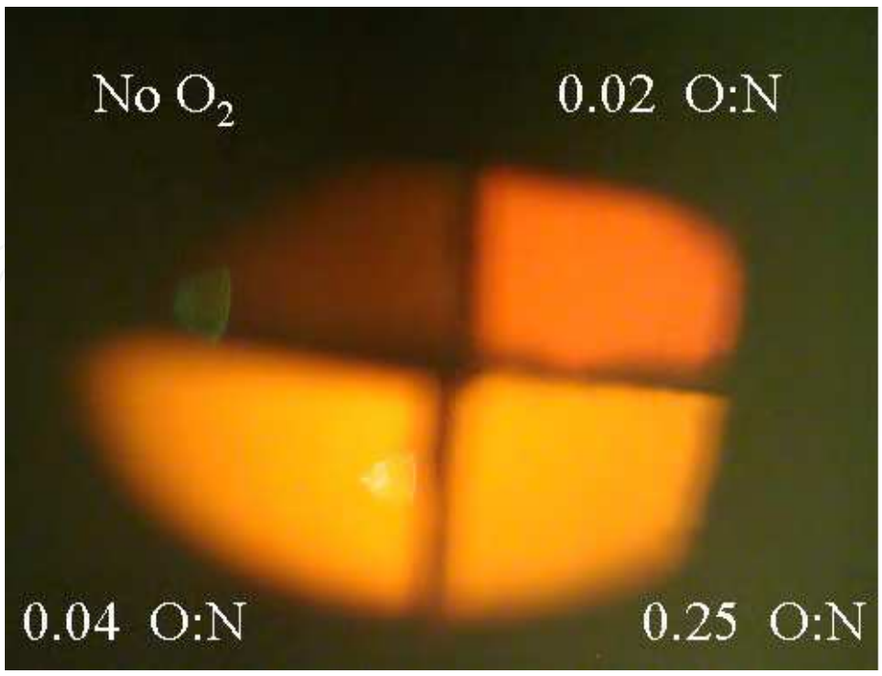

Fig. 3.11. CL from some of the types of a-AlN:Eu films described in Fig. 3.10.

3.2.2.3 Holmium and gadolinium

Data for Ho and Gd in a-AlN are given by Maqbool (Maqbool 2005).

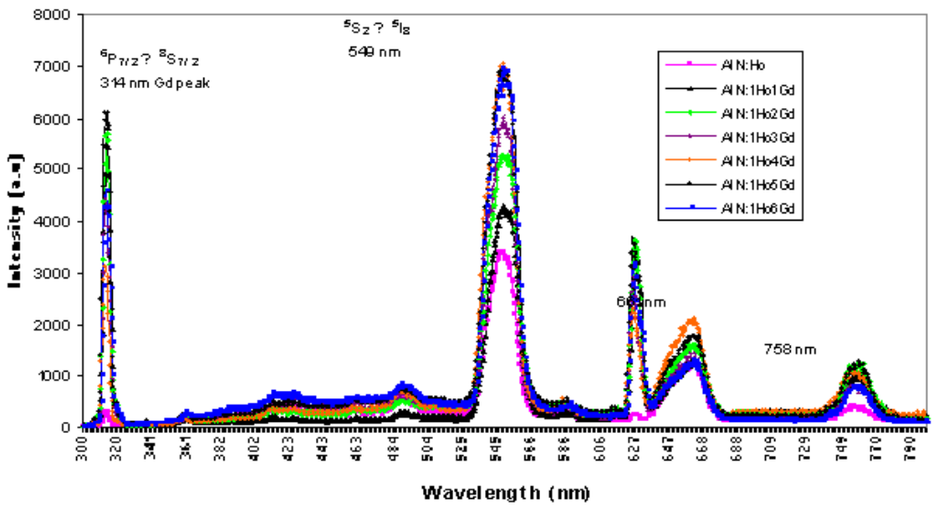

Fig. 3.12. CL from codoped Gd and Ho a-AlN films.

Material	Transition Number	Transition	Wavelength (nm)	Relative Intensity
AlN:Ho	1	$^5G_5 \rightarrow {}^5I_8$	362	0.355
	2	$^5G_4 \rightarrow {}^5I_8$	394	0.530
	3	$^5F_1 \rightarrow {}^5I_8$	461	0.300
	4	$^5S_2 \rightarrow {}^5I_8$	549	1.000
	5	$^5F_3 \rightarrow {}^5I_8$	659	0.277
	6	$^5S_2 \rightarrow {}^5I_7$	758	
AlN:Gd	1	$^6P_{7/2} \rightarrow {}^8S_{7/2}$	314	

Table 3.1. Summary of Ho^{3+} and Gd^{+3} ions emission from a-AlN:Ho and a-AlN:Gd.

Ho relative concentration	Gd relative Concentration	Relative Intensity of 549 nm peak	% increase in intensity
1	0	1	0 (reference)
1	1	1.275	27.5
1	2	1.564	56.4
1	3	1.747	74.7
1	4	2.074	107.4
1	5	2.047	104.7
1	6	2.054	105.4

Table 3.2. Effect of Gd concentration on the luminescence of Ho $^5S_2 \rightarrow {}^5I_8$ transition at 549 nm.

3.2.2.4 Praseodymium

Data for Pr in a-AlN are given by Maqbool(Maqbool 2005).

Material	Transition Number	Transition Assignment	Wavelength (nm)	Intensity(a.u)
AlN:Pr	1	$^1S_0 \rightarrow {}^1D_2$	335	162
	2	$^1S_0 \rightarrow {}^1I_6$	385	438
	3	$^3P_2 \rightarrow {}^3H_4$	439	362
	4	$^3P_0 \rightarrow {}^3H_4$	488	1002
	5	$^3P_0 \rightarrow {}^3H_4$	504	1024
	6	$^3P_1 \rightarrow {}^3H_5$	526	4577
	7	$^3P_0 \rightarrow {}^3H_5$	573	767
	8	$^3P_0 \rightarrow {}^3H_6$	618	643
	9	$^3P_0 \rightarrow {}^3F_2$	652	1227
	10	$^3P_0 \rightarrow {}^3F_3$	710	410
	11	$^3P_0 \rightarrow {}^3F_4$	738	520

Table 3.3. Summary of Pr^{3+} ion emissions from Pr-doped a-AlN.

Pr Transition	Wavelength (nm)	Gd Relative Concentration	Relative Intensity	% Increase in Intensity
$^3P_0 \rightarrow {}^3H_4$	490	0	1	0 (reference)
		1	1.58	58
		4	4.37	337
$^3P_0 \rightarrow {}^3H_6$	618	0	1	0
		1	1.73	73
		4	4.14	314
$^3P_0 \rightarrow {}^3F_2$	649	0	1	0
		1	1.66	66
		4	3.4	240

Table 3.4. Effect of Gd concentration on the luminescence of Pr^{3+} ion transitions.

3.2.2.5 Thulium

Data for Tm in a-AlN are given by Maqbool (Maqbool 2005).

Material	Transition Number	Transition Assignment	Wavelength (nm)	Relative Intensity(a.u)
AlN:Tm	1	$D_2 \rightarrow {}^3H_6$	371	0.126
	2	${}^1D_2 \rightarrow {}^3F_4$	467	1.000
	3	${}^1D_2 \rightarrow {}^3H_6$	480	0.648
	4	${}^1D_2 \rightarrow {}^3H_5$	528	0.092
	5	${}^1G_4 \rightarrow {}^3F_4$	650	0.126
	6	${}^1D_2 \rightarrow {}^3H_4$	685	0.061
	7	${}^3H_4 \rightarrow {}^3H_6$	802	0.563
	8	${}^3H_4 \rightarrow {}^3H_6$	808	0.539

Table 3.5. Summary of Tm^{3+} ion emissions from Tm-doped AlN.

3.2.2.6 Samarium

Data for Sm in a-AlN are given by Maqbool (Maqbool 2005).

Material	Transition Number	Transition Assignment	Wavelength (nm)	Relative Intensity(a.u)
AlN:Tm	1	${}^4G_{5/2} \rightarrow {}^6H_{5/2}$	564	0.425
	2	${}^4G_{5/2} \rightarrow {}^6H_{7/2}$	600	1.000
	3	${}^4G_{5/2} \rightarrow {}^6H_{9/2}$	648	0.686
	4	${}^4G_{5/2} \rightarrow {}^6H_{11/2}$	711	0.312
	5	Gd impurity	314	0.276
	6	Cr impurity	692	0.220

Table 3.6. Summary of Sm^{3+} ion emissions from Sm-doped a-AlN.

3.2.3 Amorphous gallium nitride

Amorphous GaN usually has a large defect luminescence in the yellow region of the visible spectrum. In Fig. 3.13, an a-GaN:Er thin film is shown in CL. This film was heated to 950 ^oC in nitrogen for 30 minutes. The Er^{3+} ion transitions are clearly visible on the yellow defect emission band. The defect band problem is much less in crytsalline GaN, which was extensively investigated by several groups, most notably Steckl and his coworkers.

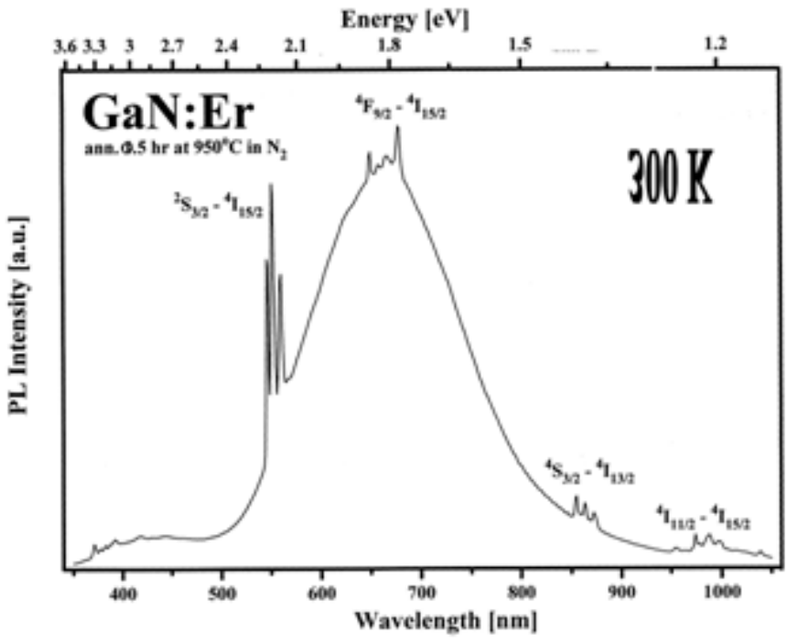

Fig. 3.13. CL from a-GaN: Er.

Maqbool (Maqbool, Richardson et al. 2005) investigated Pr^{3+} ion luminescence in a-GaN. The data are given in Table 3.7 .

Material	Transition Number	Transition Assignment	Wavelength (nm)	Relative Intensity(a.u)
	3	$^3P_2 \rightarrow {}^3H_4$	418	559
	4	$^3P_0 \rightarrow {}^3H_4$	493	5687
	6	$^3P_1 \rightarrow {}^3H_5$	532	1895
	8	$^3P_0 \rightarrow {}^3H_6$	621	4015
	9	$^3P_0 \rightarrow {}^3F_2$	650	4227
	10	$^3P_0 \rightarrow {}^3F_3$	713	1508
	11	$^3P_0 \rightarrow {}^3F_4$	736	1627

Table 3.7. GaN:Pr

3.2.4 Other amorphous nitrides

3.2.4.1 BN

Sputtered boron nitride was shown to be a useful host for RE ions by Maqbool et al. (Maqbool, Richardson et al. 2005) and Allen et al. (Allen S. 2000).

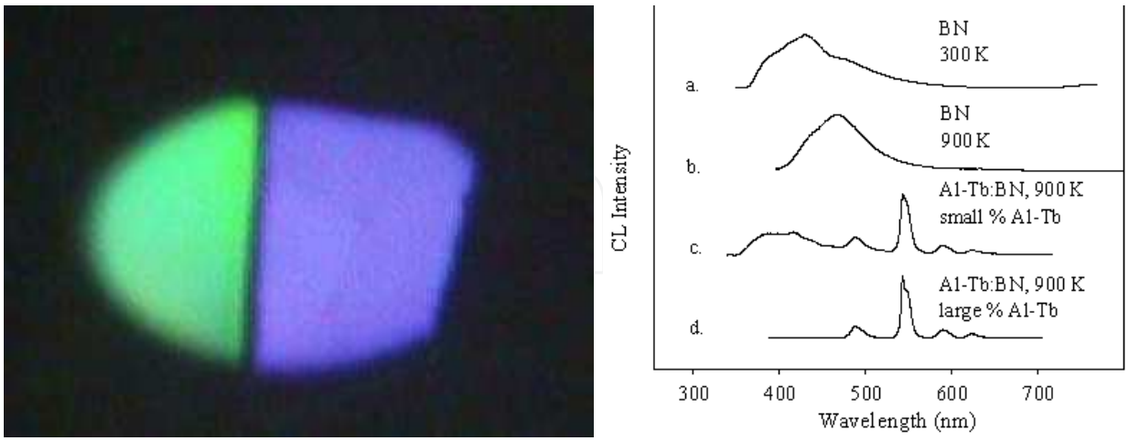

Fig. 3.14. Left: CL from sputter deposited BN:Tb and pure BN. Right: CL spectra of BN and BN:Tb, as deposited and heated to 900 K. At large Tb concentrations, the blue BN luminescence is not visible.

Maqbool et al. (Maqbool, Richardson et al. 2005) investigated the luminescence of Pr in BN.

Data are given below in Table 3.8 (Maqbool 2005)

Material	Transition Number	Transition Assignment	Wavelength (nm)	Relative Intensity(a.u)
	3	BN transition	415	372
	4	$^3P_0 \rightarrow {}^3H_4$	492	973
	6	$^3P_1 \rightarrow {}^3H_5$	544	752
	8	$^3P_0 \rightarrow {}^3H_6$	628	842
	9	$^3P_0 \rightarrow {}^3F_2$	651	748
	10	$^3P_0 \rightarrow {}^3F_3$	713	257
	11	$^3P_0 \rightarrow {}^3F_4$	736	289

Table 3.8. BN:Pr

3.2.4.2 BeN

Amorphous Beryllium Nitride, produced by reactive sputtering of Be in nitrogen, was studied with samarium (Zanatta, Richardson et al. 2007).

PL and CL excitation was achieved with 532 nm photons and 10 keV electrons, respectively. Light emission is due to the Sm^{3+} ions and correspond to the following transitions (see inset on the left in Fig. 3.15): $^4G_{5/2} \rightarrow {}^6H_{5/2}$ (A), $^4G_{5/2} \rightarrow {}^6H_{7/2}$ (B), $^4G_{5/2} \rightarrow {}^6H_{9/2}$ (C), and $^4G_{5/2} \rightarrow {}^6H_{11/2}$ (D). A photograph illustrating the cathodoluminescence image of the Sm-doped a-BeN sample is presented in the upper-right corner of Fig. 3.15.

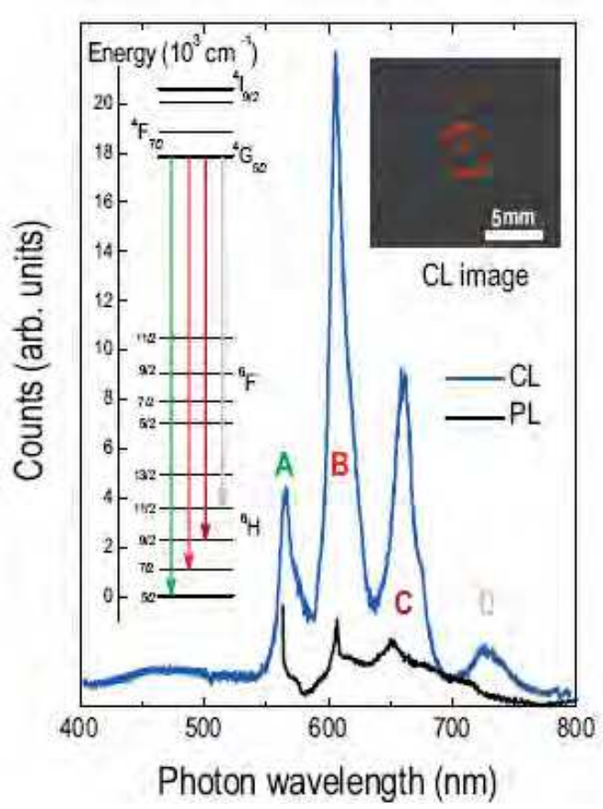

Fig. 3.15. Room-temperature luminescence spectra of a Sm-doped a-BeN film. From(Zanatta, Richardson et al. 2007)

4. Transition metal cathodoluminescence

Elements in the periodic table that make a bridge between the first two groups and last six groups of the main elements are defined as transition metals (TM). This bridging role has given these elements the name *transition* metals. These metals consist of many elements, however, we shall limit our discussion to a few of them, mainly $_{22}$Ti, $_{24}$Cr, $_{39}$Y, and $_{74}$W . These metals are specially characterized by their common feature: partial occupancy of the d-shells. This partially filled *d* shell configuration assigns special properties to these elements, including their strong suitability for use as optical and luminescent materials. To study their optical and luminescent properties it will be useful to understand some of their basic characteristics. Housecroft (Housecroft et al 2007) and Mackay (Mackay 1996) reported some of the basic characteristics of transition metals. The discussion of these characteristics in section 4.1 follows Housecroft and Mackay.

4.1 Characteristics of transition metals

4.1.1 Density and metallic radii

The transition elements are much denser than the s-block elements and show a gradual increase in density from scandium to copper. This trend in density can be explained by the small and irregular decrease in metallic radii coupled with the relative increase in atomic mass.

4.1.2 Melting and boiling points

The melting points and the molar enthalpies of fusion of the transition metals are both high in comparison to main group elements. This arises from strong metallic bonding in transition metals which occurs due to delocalization of electrons facilitated by the availability of both d and s electrons.

4.1.3 Ionization energies

In moving across the series of metals from scandium to zinc a small change in the values of the first and second ionization energies is observed. This is due to the build-up of electrons in the immediately underlying d-sub-shells that efficiently shields the 4s electrons from the nucleus and minimizing the increase in effective nuclear charge from element to element. The increases in third and fourth ionization energy values are more rapid. However, the trends in these values show the usual discontinuity half way along the series. The reason is that the five d electrons are all unpaired, in singly occupied orbitals. When the sixth and subsequent electrons enter, the electrons have to share the already occupied orbitals resulting in inter-electron repulsions, which would require less energy to remove an electron. Hence, the third ionization energy curve for the last five elements is identical in shape to the curve for the first five elements, but displaced upwards by 580 kJ mol^{-1}.

4.1.4 Electronic configuration

The electronic configuration of the atoms of the first row transition elements are basically the same. It can be seen in Table 4.1 that there is a gradual filling of the 3d orbitals across the series starting from scandium. This filling is, however, not regular, since at chromium and copper the population of 3d orbitals increase by the acquisition of an electron from the 4s shell. This illustrates an important generalization about orbital energies of the first row transition series. At chromium, both the 3d and 4s orbitals are occupied, but neither is completely filled in preference to the other. This suggests that the energies of the 3d and 4s orbitals are relatively close for atoms in this row.

In the case of copper, the 3d level is full, but only one electron occupies the 4s orbital. This suggests that in copper the 3d orbital energy is lower than the 4s orbital. Thus the 3d orbital energy has passed from higher to lower as we move across the period from potassium to zinc. However, the whole question of preference of an atom to adopt a particular electronic configuration is not determined by orbital energy alone. In chromium it can be shown that the 4s orbital energy is still below the 3d which suggests a configuration $[Ar]3d^4 4s^2$. However due to the effect of electronic repulsion between the outer electrons the actual configuration becomes $[Ar]3d^5 4s^1$ where all the electrons in the outer orbitals are unpaired. Table 1 gives some of the physical properties and free atom electronic configuration of transition metals.

4.1.5 Oxidation states

Oxidation states of transition metals are very important to study the spectroscopy and luminescence from these metal ions. The partially filled d-shell electrons play important role in the oxidation states of transition metals. To fully understand the phenomena of

oxidation states of transition metals, we have to understand how the unpaired d-orbital electrons bond. There are five orbitals in a d subshell manifold. As the number of unpaired valence electrons increases, the d-orbital increases, the highest oxidation state increases. This is because unpaired valence electrons are unstable and eager to bond with other chemical species. This means that the oxidation states would be the highest in the very middle of the transition metal periods due to the presence of the highest number of unpaired valence electrons. To determine the oxidation state, unpaired d-orbital electrons are added to the 2s-orbital electrons since the 3d-orbital is located before the 4s-orbital in the periodic table. For example: Scandium has one unpaired electron in the d-orbital. It is added to the 2 electrons of the s-orbital and therefore the oxidation state is +3. So that would mathematically look like: 1s electron + 1s electron + 1d electron = 3 total electrons = oxidation state of +3.

The formula for determining oxidation states would be (with the exception of copper and chromium):

$$\textit{Highest Oxidation State for a Transition metal} = \\ = \textit{Number of Unpaired } d-\textit{electrons} + \textit{Two } s-\textit{orbital electrons}$$

Element	Group	Density (g/cm^3)	M.P. (°C)	B.P. (°C)	Radius (pm)	Free atom configuration	ionization energy ($kJ\ mol^{-1}$)	Oxidation state
Sc	3	2.99	1541	2831	164	[Ar] $3d^1 4s^2$	631	+3
Ti	4	4.50	1660	3287	147	[Ar] $3d^2 4s^2$	658	+2, +3, +4
V	5	5.96	1890	3380	135	[Ar] $3d^3 4s^2$	650	+2, +3, +4, +5
Cr	6	7.20	1857	2670	129	[Ar] $3d^5 4s^1$	653	+2, +3, +6
Mn	7	7.20	1244	1962	137	[Ar] $3d^5 4s^2$	717	+2, +3, +4, +6, +7
Fe	8	7.86	1535	2750	126	[Ar] $3d^6 4s^2$	759	+2, +3
Co	9	8.90	1495	2870	125	[Ar] $3d^7 4s^2$	758	+2, +3
Ni	10	8.90	1455	2730	125	[Ar] $3d^8 4s^2$	737	+2
Cu	11	8.92	1083	2567	128	[Ar] $3d^{10} 4s^1$	746	+2
Zn	12	7.14	420	907	137	[Ar] $3d^{10} 4s^2$	906	+2

Table 4.1. Physical properties and free atom electronic configuration of transition metals.

Scandium is one of the two elements in the first transition metal period which has only one oxidation state (zinc is the other, with an oxidation state of +2). All the other elements have at least two different oxidation states. Manganese, which is in the middle of the period, has the highest number of oxidation states, and indeed the highest oxidation state in the whole period since it has five unpaired electrons.

It was mentioned previously that both copper and chromium do not follow the general formula for transition metal oxidation states. This is because copper has 9 d-electrons, which would produce 4 paired d-electrons and 1 unpaired d-electron. Since copper is just 1 electron short of having a completely full d-orbital, it steals an electron from the s-orbital, allowing it to have 10 d-electrons. Likewise, chromium has 4 d-electrons, only 1 short of having a half-filled d-orbital, so it steals an electron from the s-orbital, allowing chromium to have 5 d-electrons.

4.2 Luminescence from pure TM doped in nitride semiconductors

Luminescence and spectroscopic properties of materials play an important role in optical device fabrication, display technologies and the laser industry; transition metals are not exceptions. The optical properties of transition metal ion solids have been studied for many years. Hidalgo (Hidalgo, Mendez et al. 1998) and Muller (Muller, Zhou et al. 2009) studied that partially occupied d-shells of these elements play important role in the luminescence and spectroscopy of these elements. Thurbide (Thurbide and Aue 2002), Gedam (Gedam, Dhoble et al. 2007), Grinberg (Grinberg, Barzowska et al. 2001) and Lapraz (Lapraz, Iacconi et al. 1991) reported that in many host materials, these partially occupied d-shells give rise to several important technological applications and in particular, production of high resistivity materials and photonic devices through transition-metal doping has been widely used. Maqbool (Maqbool, Wilson et al. 2010) and Martin (Martin, Spalding et al. 2001) showed that thermal activation, the oxygen effect and co-dopants are good tools to obtain high efficiency and improved luminescence from these metal ions.

Recent progress toward nitride-based light-emitting diodes and electroluminescent devices (ELDs) has been made using crystalline and amorphous nitride semiconductors doped with a variety of transition metals: Richardson (Richardson, Van Patten et al. 2002), Maqbool (Maqbool, Main et al. 2010; Maqbool, Wilson et al. 2010) and Caldwell (Caldwell, Martin et al. 2001). The amorphous III-nitride semiconductors are equally important as their crystalline counterpart because the amorphous material can be grown at room temperature with little stress due to lattice mismatch. They may also be more suitable for waveguides and cylindrical and spherical laser cavities because of the elimination of grain boundaries at low temperature growth. Cathodoluminescence, spectroscopy and the effects of various factors on the luminescence of a few TMs are given below.

4.2.1 Chromium doped in amorphous aluminum nitride

Thin films of a-AlN:Cr were prepared and deposited on Si (100) substrate by the method of plasma magnetron sputtering at low temperature as described earlier. The x-ray diffraction (XRD) analysis confirmed that the deposited films were amorphous.

Figure 4.1 shows the XRD analysis of the a-AlN:Cr films deposited on flat Si(100) substrate. Only one peak can be observed in the film at 69.1° which corresponds to Si(100). No other peak is present in the figure, indicating that the films deposited on flat silicon substrates are amorphous. Thermal activation of the films at 1200 K has not changed the structure of the films.

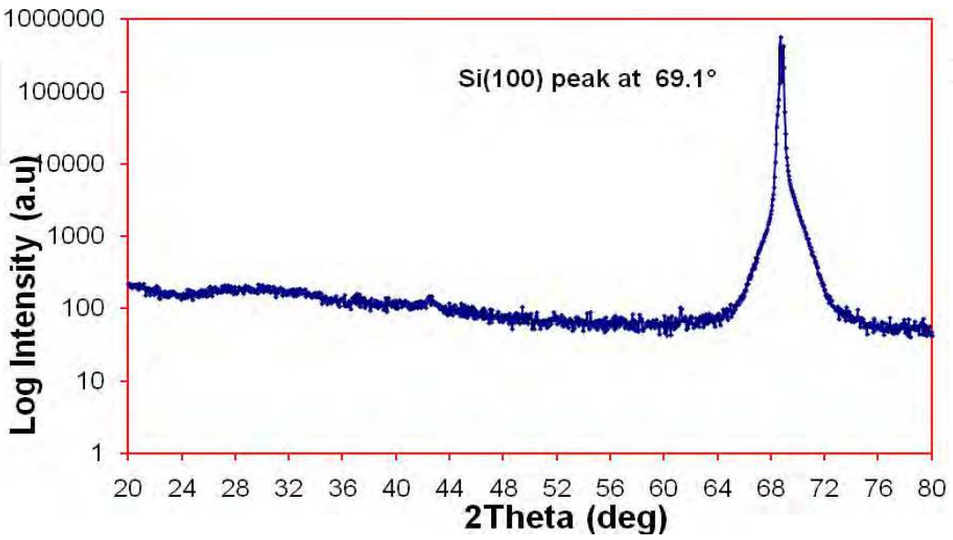

Fig. 4.1. XRD analysis of the a-AlN:Cr films deposited on flat Si (100) substrate.

Cathodoluminescence (CL) of the Cr-doped a-AlN was obtained to study the suitability of this TM for various applications in optical and display technology. Figure 4.2 shows the CL spectrum of the as-deposited and thermally activated a-AlN:Cr in 600 nm to 750 nm range.

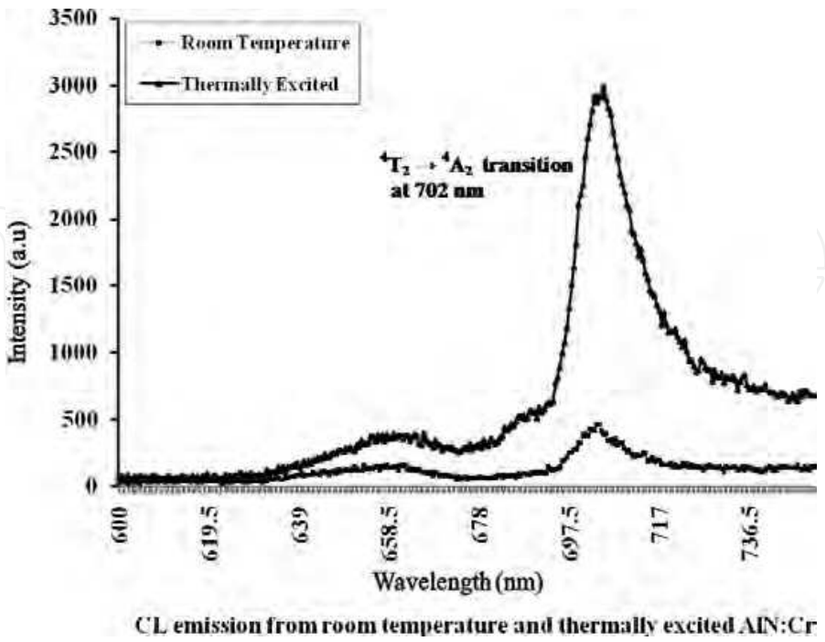

Fig. 4.2. CL spectra of room temperature and thermally activated a-AlN:Cr films.

A strong emission has occurred at 702 nm indicated by a sharp peak in Fig. 4.2. This peak corresponds to $^4T_2 \rightarrow {}^4A_2$ transition. It is clear from the figure that thermal activation enhances the luminescence intensity six times. A small peak at 661 nm is also observed. This peak corresponds to Ho^{+3} ion, indicating the presence of holmium impurity in the films.

Figure 4.2 reports that the intensity of the emission is not only strong but an enhancement in the luminescence is possible by various means like thermal activation. The strong intensity enabled us to see the red emission in CL apparatus directly with naked eye when the excitation current is reasonably high. Six times increase in the emitted light intensity makes it possible that a-AlN:Cr can serve as a potential candidate for a laser production at 702 nm and other optical devices applications. Moreover the significant increase in the intensities of luminescence from Cr^{+3} ions by thermal activation can be explained on the basis of luminescence from the triply ionized chromium ions. Luminescence occurs from Cr^{+3} ions and not from Cr^{+2} or Cr^{+1}. During the film deposition it is most likely that some of Al^{+3} of AlN may be replaced by Cr^{+3} but there are also chances for imperfections and defects giving rise to Cr^{+2} and Cr^{+1}during film growth. These ions do not contribute to luminescence. The smaller the number of these ions, more will be Cr^{+3} ions and hence luminescence will be higher. When these films are activated thermally at a higher temperature then most of Cr^{+2} and Cr^{+1} impurities ionize and convert to Cr^{+3} ions giving a path to enhanced luminescence. Moreover when the films are transferred to the furnace and thermally activated after removed from the deposition chamber, they are exposed to air. Thus oxidation of the surface of the film cannot be ignored. Oxygen enhances the luminescence of TM ions giving rise to the enhanced luminescence after thermal activation of the films. Chen (Chen, Chen et al. 2000), Little and Kordesch (Little and Kordesch 2001) and Suyver (Suyver et al. 2005) have reported such results in other materials as well.

The results show that amorphous AlN:Cr is a promising candidate for its use in optical and photonic devices and communication tools. The strong red-IR emission makes this material a potential candidate for making laser cavities, quantum dots and other wave-guided applications. Due to the high penetration ability of near infrared light in human tissues, it can also be used in biomedical applications.

4.2.2 Tungsten doped in amorphous aluminum nitride

Another important member of the TM family is Tungsten (W). Tugsten has the highest melting point and lowest vapor pressure of all metals. It has a very high tensile strength. Our investigations revealed that along with other physical properties tungsten can also be used for visible light emission applications. The cathodoluminescence of tungsten shows that it gives a very broad emission under cathode ray excitation. The emission spectrum is so broad that it covers the entire visible range of the electromagnetic spectrum from 350 nm up to 700 nm. However the dominant portion of the spectrum comes in blue region with a peak at 491 nm. Another peak in blue is also observed at 429 nm. Because of the huge portion of the spectrum and its peaks lying in blue the films also looked blue in appearance when directly exposed to the electron beam in CL. This broad CL emission from tungsten is shown in Fig. 4.3.

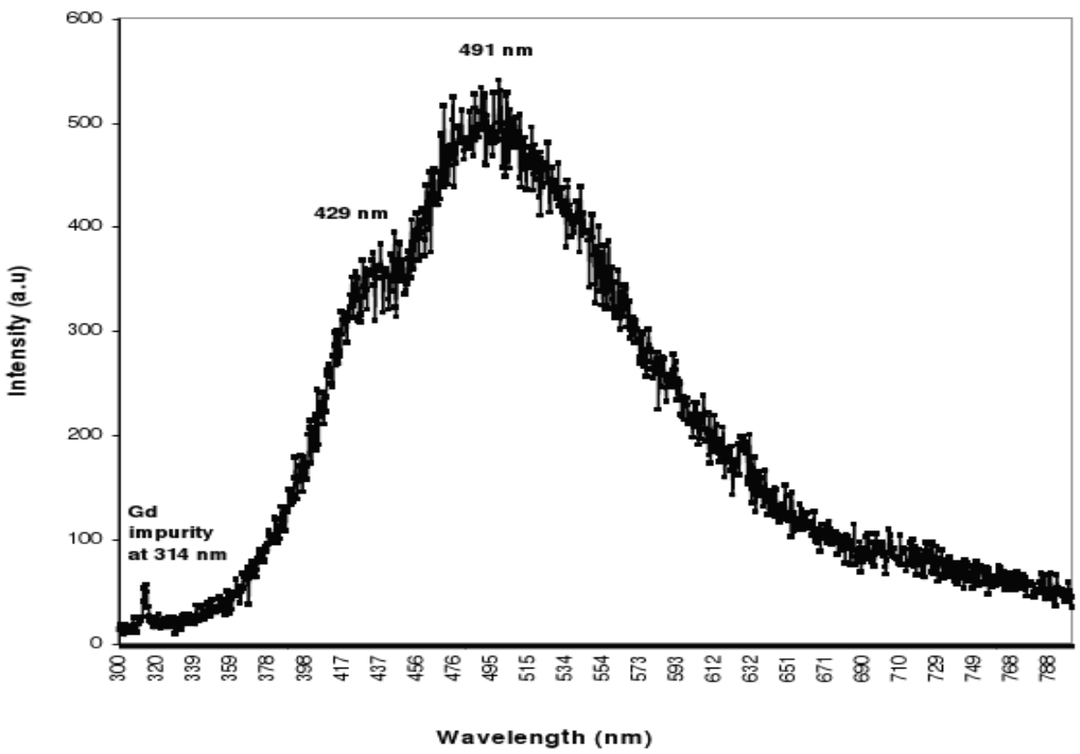

Fig. 4.3. CL spectrum of amorphous AlN:W

4.2.3 Interaction of co-doped Gd^{+3} with AlN:W

Due to its broad emission W^{+3} is also able to interact with other ions when co-doped with it. For this purpose it was also co-doped with holmium and gadolinium separately to test for

luminescence enhancement in the green emission from holmium ions or luminescence enhancement in the AlN:W by gadolinium. It was observed that no change has occurred in Ho luminescence by the addition of W. However the luminescence from Gd has enhanced W luminescence. Figure 4.4 shows how the addition of Gd^{+3} affects the light emission from W^{+3}.

Figure 4.4 shows luminescence from amorphous AlN films co-doped with 1 piece of W and 1-3 pieces of Gd. It is clear from the figure that the addition of Gd has a dominant effect on the luminescence from W. Luminescence from AlN:1W2Gd is 3 times the luminescence from AlN:1W1Gd and luminescence from AlN:1W3Gd is almost 6 times the luminescence from AlN:1W1Gd. This fact shows a huge increase in intensities in the W luminescence by Gd.

Figure 4.4 also reveals some other information. It can be observed that the main peak in blue shifts with the relative increase in Gd concentration. With one piece of Gd the main peak of W appears at 506 nm. With two pieces of Gd added to AlN:W the peak gets bigger but shifts to 534 nm. However with the addition of another piece of Gd the peak gets bigger but shifts back to 523 nm. A possible explanation for this shift in the peaks may be the activation of new radiative energy levels in W by the Gd. Further, the intensity of Gd peak is reduced with higher concentration of Gd. Table 4.2 is giving the increase in the W intensity with the concentration of Gd and also the intensity of Gd peak with the concentration of Gd.

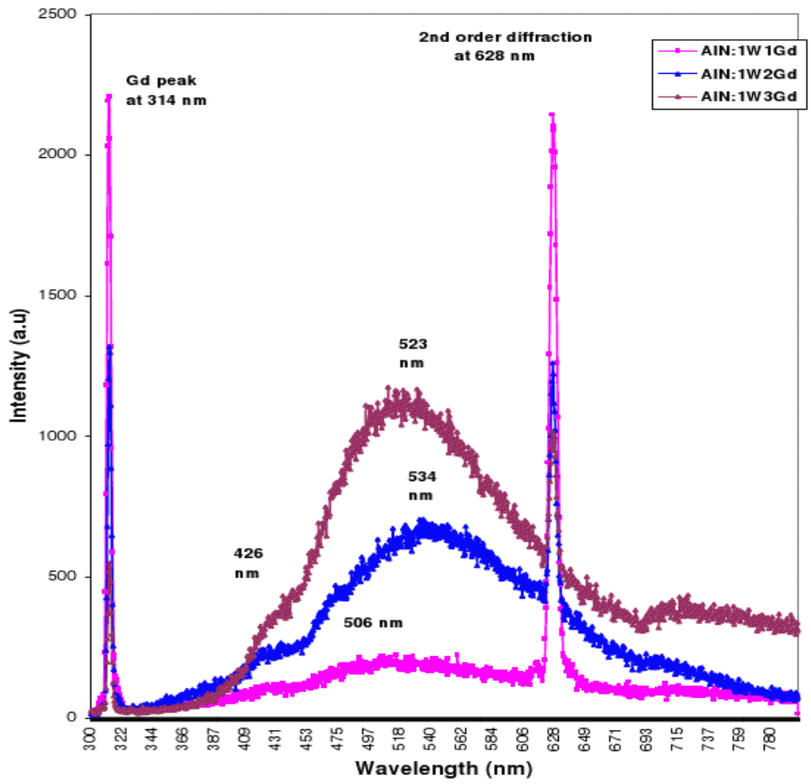

Fig. 4.4. The effect of Gd concentration on the luminescence of a-AlN:W films.

4.2.4 Interaction of co-doped Ho^{+3} with AlN:W

Tungsten is added to Holmium (Ho) in order to observe any enhancement in the green luminescence from Ho. Figure 4.5 shows the effect of varying W concentration on Ho. A comparison between amorphous AlN:1Ho1W, AlN:1Ho3W and thermally activated AlN:1Ho1W is given in this figure. It is clear from the figure that there is no effect of increasing W concentration on the Ho luminescence. The W concentration is increased 3 times which made the W peak broad but no enhancement in Ho. Further, if we compare this figure with the pure W spectrum then a shift can be seen in the W emission wavelength just like that happened due to Gd. And we see from the figure that in the presence of Ho, tungsten emits a single blue light with a wavelength of 461 nm rather than emissions at 429 nm and 491 nm in pure tungsten. A possible explanation may be the holmium has affected the energy level distribution in tungsten. Further it can also be given in explanation that this shift of wavelength did not occur in rare-earth elements discussed in previous chapters but the transition element W has suffered a lot from this shift. Since rare-earth elements are favorable for their internal f-f transitions. These f-levels lying inside the other shells and hence any external change barely affect these transitions. However it is not true for transition metals and they can be significantly affected by other dopant impurities. Moreover this figure also gives us the effect of thermal annealing on the luminescence of W and Ho. It can be easily deduced from the figure that thermal annealing has activated Ho luminescence more than W. There is also existence of a ruby impurity, which is considerably enhanced in luminescence by thermal activation.

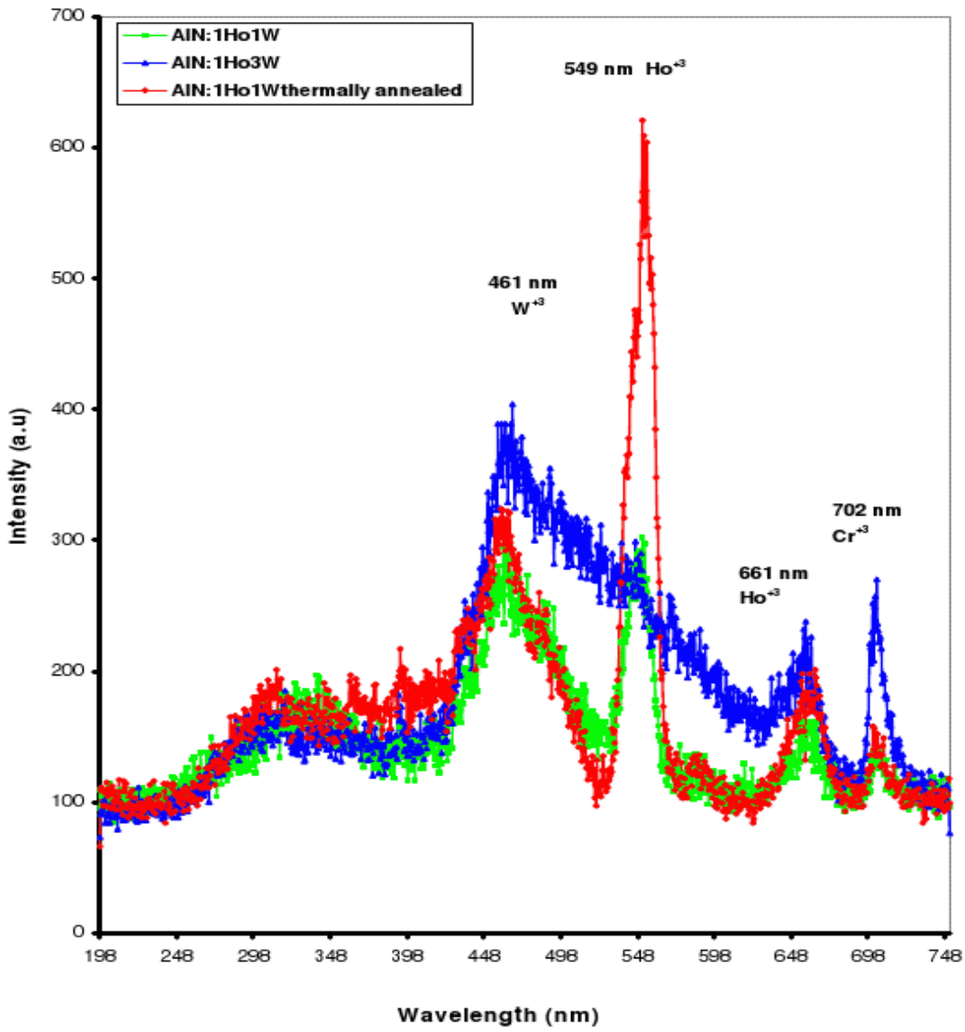

Fig. 4.5. The effect of thermal activation and W concentration on Ho luminescence.

Gd Concentration	Intensity of Gd luminescence (a.u)	Intensity of W luminescence (a.u)	Percent increase in luminescence of W
1	2207	208	Reference
2	1318	705	339
3	538	1159	557

Table 4.2. The effect of Gd^{+3} concentration on the W and Gd emission.

4.2.5 Cathodoluminescence and thermal activation of AlN doped with Yttrium (Y)

Cathodoluminescence of cold deposited Yttrium doped AlN films were characterized for CL in the same way described earlier for other materials. Figure 4.6 represents the luminescence from AlN:Y films when exposed to cathode rays in CL assembly. This figure confirms emission from amorphous AlN:Y films in UV , blue and in bluish green regions. There is also a peak in IR which may correspond to Yttrium or possibly a ruby impurity. The wavelengths correspond to these emissions are 360 nm, 421 nm, 518 nm and 705 nm respectively. The emission 705 nm could be from AlN:Y or from Cr^{+3} The bluish green and blue emissions are the dominant in intensity and that is why the films appear blue to naked eye when exposed to electron beam in CL. However we already know from the previous materials investigations that thermal annealing tremendously enhance the luminescence from Cr^{+3} and hence we can analyze this peak obtaining the CL after performing thermal annealing.

Figure 4.7 gives a comparison of CL spectra from amorphous AlN:Y before and after thermal activation. Films were thermally activated at 900 °C for one hour and then characterized for CL. From the figure it is clear that thermal activation has almost no effect on the Yttrium luminescence at 360 nm, 421 nm and 518 nm. However the peak at 705 nm is strongly enhanced by thermal activation. This enhancement in the peak at 705 nm is more than three and half times the luminescence from the same peak in the film, which is not thermally activated. Further, this peak was less than half the intensity of peak at 518 nm before thermal activation but after activation it is about one and half time more intense than the peak at 518 nm. One can guess at this stage that the peak at 705 is most probably due to chromium oxide (Ruby) rather than emission from yttrium ions itself.

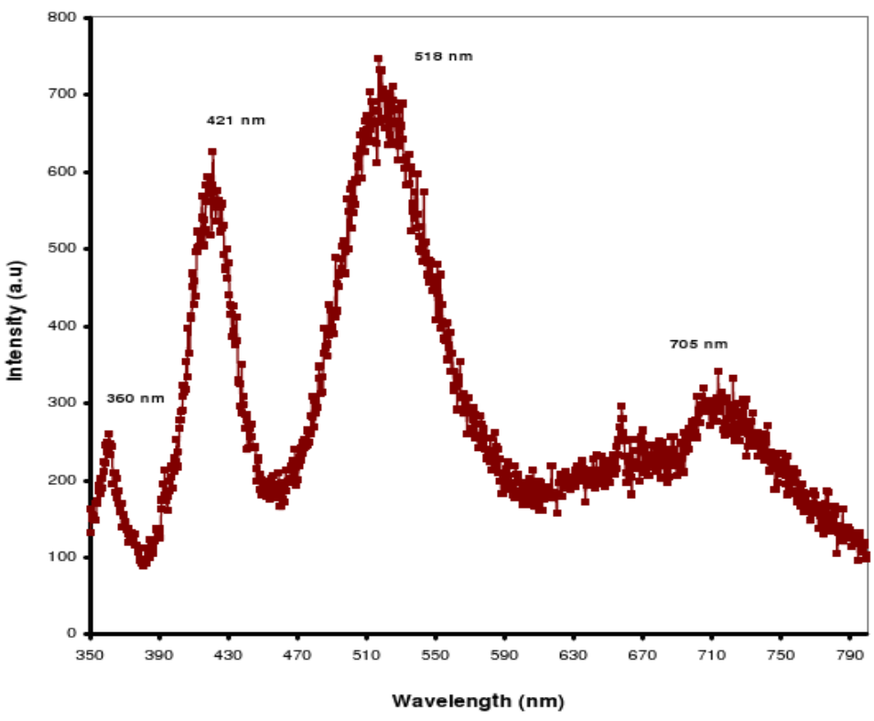

Fig. 4.6. CL spectrum of amorphous AlN:Y

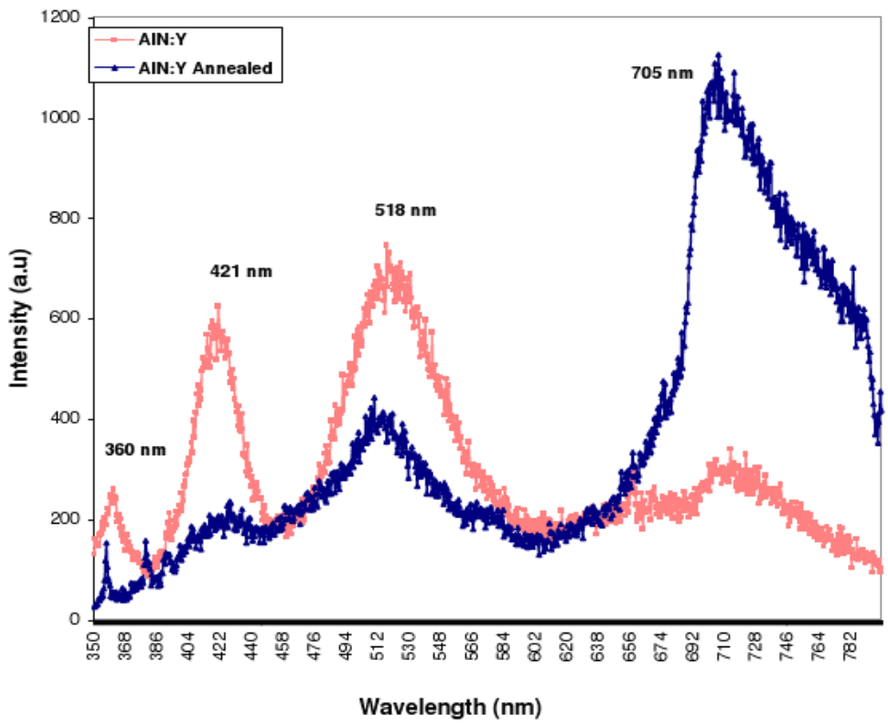

Fig. 4.7. Comparison of the CL spectra of thermally activated and as deposited amorphous AlN:Y films.

4.2.6 Titanium doped amorphous aluminum nitride

Titanium is one of the important members of the TM family. It is lightweight, strong, corrosion resistant metal and the ninth most plentiful amongst all the elements in the earth's crust. This metal, when doped in nitride semiconductors, is proved to be a very good source to make laser cavities and optical devices. The cathodoluminescence of Ti^{+3} doped in amorphous AlN shows a broad emission over a wide range from 650 nm up to 900 nm with a peak around 760 nm. Figure 4.8 shows the CL spectrum of a-AlN:Ti. The broad emission is clear from the spectrum.

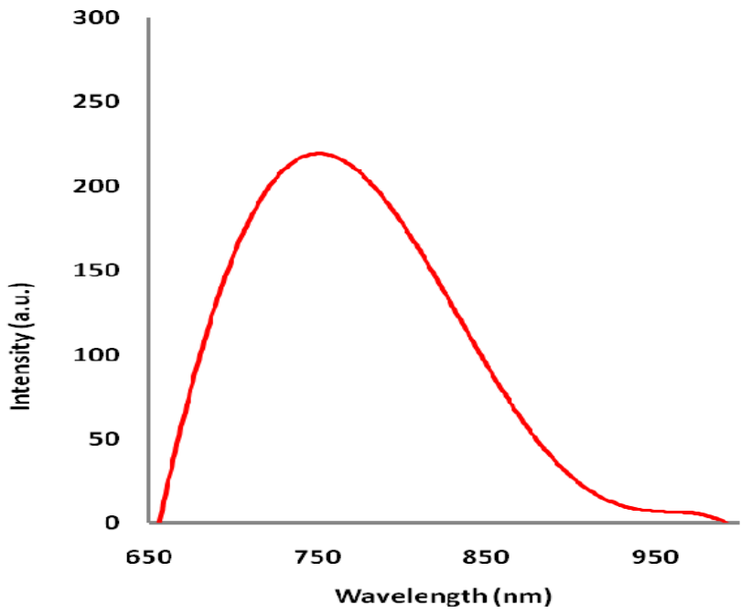

Fig. 4.8. Cathodoluminescence spectrum of amorphous AlN:Ti.

5. Applications and special geometries

5.1 Amorphous AlN:Tm (Ti) on optical fiber in a cylindrical and ring geometry

The broad emission from a-AlN:Ti, as discussed in the previous section, makes it hard to use it directly for any particular wavelength application. However it has a great potential for narrowing the peak by a resonance emission to produce a laser out of Ti^{+3}. The resonance emission to produce a laser will definitely need a cavity. Rather than making a traditional cavity, however, we made a cavity by depositing a-AlN:Ti, around optical fiber and obtained a microlaser with emission wavelength of 780.5 nm. The fiber acts as a cavity when the light emitted from the deposited film circulates around the fiber. Only those light waves will enhance each other whose wavelength is an integral multiple of their path around the fiber.

Figure 5.1 represent thin film deposition and light propagation around optical fiber, where 5.1(a) shows longitudinal view of the fiber containing thin film around it. The dark red region around the fiber is the a-AlN:Ti, film deposited uniformly around the fiber. Figure 5.1(b) is a cross sectional view of the fiber with the film, showing light propagation in whispering gallery mode (WGM), The diameter 's' of this section is 12 μm. The dark red region around the fiber is the a-AlN:Ti film deposited on the fiber. The thickness 'd' of this film is 4 micron. This makes the total diameter of the fiber and the film around it to be 20 micron (D = 2d + s = 20 μm). The white lines in the film represent the propagation of light in the film. The pattern of light propagation is restricted to the a-AlN:Ti film only, without touching the fiber itself. Such arrangement is known as whispering gallery. Figure 5.1(c) shows pump laser coupled to fiber and microring emission. Optical fiber with a-AlN:Ti film was held such that it's longitudinal axis is perpendicular to the pump laser beam direction. The pump laser hits the thin films around the fiber directly, exciting a-AlN:Ti for infrared emission, that generates whispering gallery modes in the fiber. The laser produced in the fiber cavity comes out as a microring emission from the fiber.

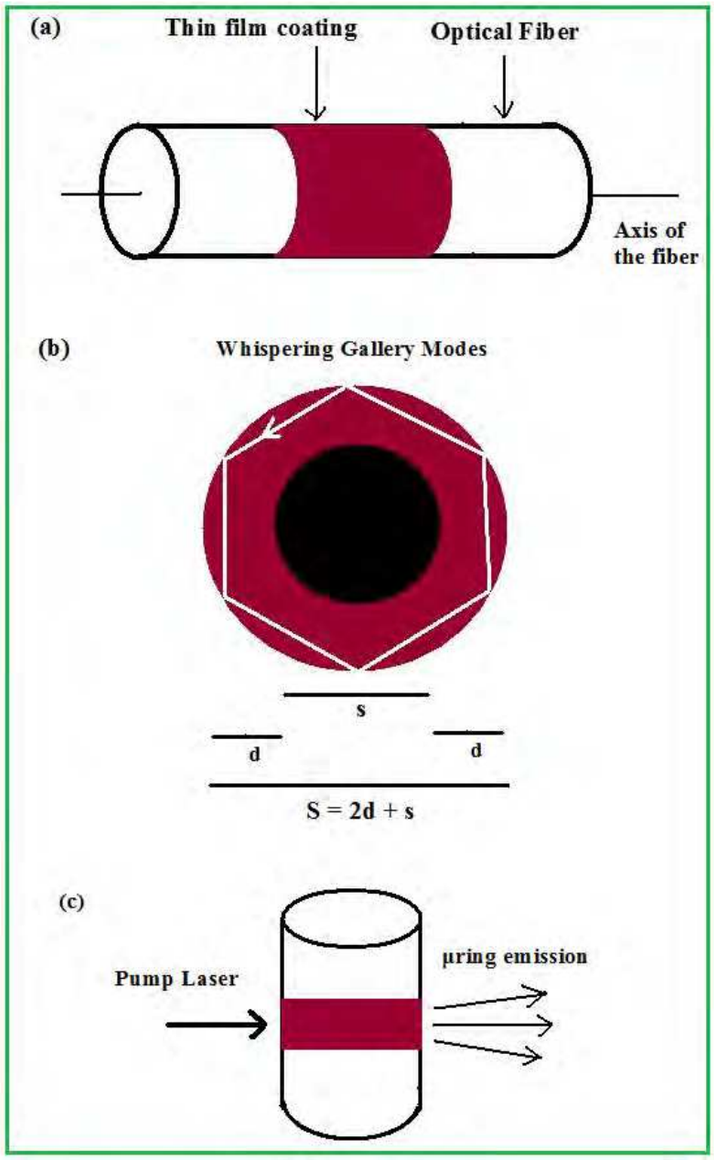

Fig. 5.1. Whispering gallery mode microlaser cavity formation around optical fiber.

Figure 5.2 shows the band narrowing and laser action in a-AlN:Ti films deposited around the optical fiber excited by 532 nm Nd:YAG laser. The power of the excitation laser is varied between 7.5 mW and 30 mW. The figure shows two emission spectra. The broad spectrum showing just the fluorescence emission from the deposited films was obtained when 15 mW of power from the Nd:YAG laser is used for excitation. This broad emission spectrum is about 20 nm wide and no lasing action is observed in this spectrum under 15 mW excitation power. The sharp and very intense emission with narrow bandwidth shows lasing action in the film. The laser is produced in the whispering gallery mode at 780.5 nm. We also observed the secondary modes in this spectrum, confirming the resonances in the lasing action. The primary mode lasing and the secondary mode emission peak show gain of ~ 20 at an input power around 30 mW.

Figure 5.3 gives increase in the observed near infrared laser in a-AlN:Ti with the increasing power of Nd:YAG pump laser. The curve shows that no laser action can be achieved in a-AlN:Ti if the power P of excitation laser is less than a threshold value P_0 . For $P > P_0$ an almost linear increase in the titanium microlaser emission was observed with increasing excitation laser power. The threshold power P_0 was found to be about 23.5 mW. For $P < P_0$ we just observed a fluorescence emission from the fiber with an emission width of 35 nm.

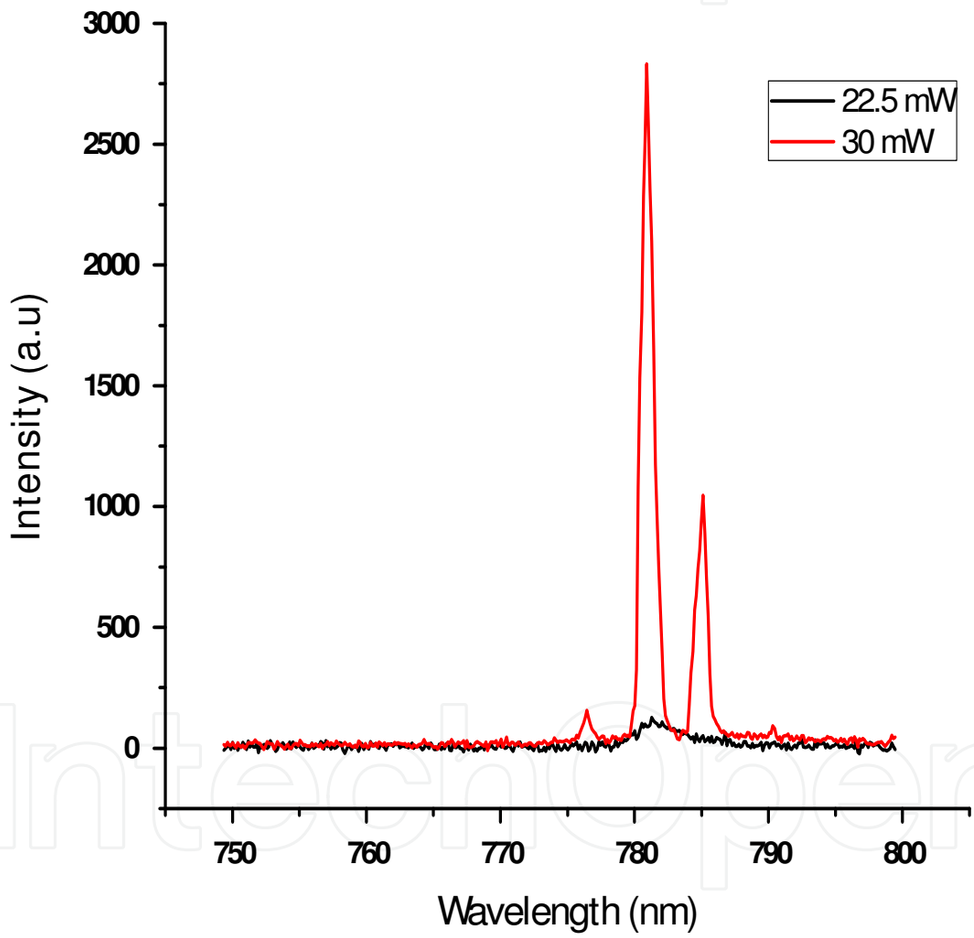

Fig. 5.2. Laser action at 780.5 nm in a-AlN:Ti thin films around optical fiber. The Equally spaced peaks at 776.4 nm and 785.5 nm are the secondary modes of laser. Mode spacing is 4.6 nm.

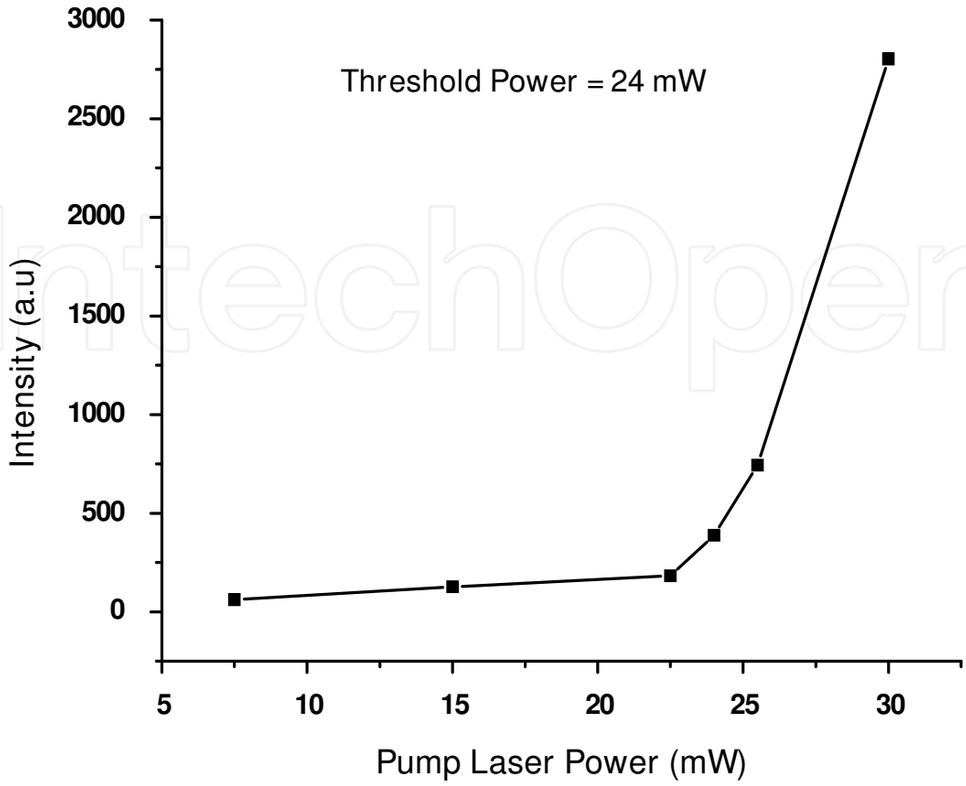

Fig. 5.3. Increase in the a-AlN:Ti laser intensity with the pump laser power. A threshold power of 24 mW can be observed.

In micro-ring cavities, the thin a-AlN:Ti film deposited around the optical fiber supports whispering gallery modes. Frolov (Frolov, Fujii et al. 1998) (Frolov, Vardeny et al. 1998) and Maqbool and Kordesch (Maqbool, Main et al. 2010) figured out that the angular momentum mode number (n) for a WGM is given by equation (1), where D is the diameter of the optical fiber with thin film deposited on it, λ_n is the wavelength of the WGM and m is the index of refraction for the a-AlN film.

$$n = \pi D m / \lambda_n \quad (1)$$

Khoshman and Kordesch (Khoshman and Kordesch 2005) worked on amorphous AlN and found that the refractive index in the near infrared region (780.5 nm) is 1.95. This value of the index of refraction of amorphous AlN is obtained using the films deposited in the same deposition system and the same conditions that we used for our work. Thus, m = 1.95 is the most appropriate value to use in our work. Our results satisfy the given equation for the integers n = 157. Because the film around the optical fiber is thick enough to satisfy the WGM condition ($d/D \geq 0.2$), we did not observe waveguide modes. The a-AlN:Ti doped optical fiber was placed in vertical direction so that the ring laser formation occur in a horizontal axis. The resonance wavelength λ_n should also support the mode separation $\Delta\lambda$ equation, given by;

$$\Delta\lambda = \lambda_n - \lambda_{n+1} = \lambda^2 / \pi D m \quad (2)$$

Using n = 156, the outer diameter D = 20 micron, and m = 1.95, equation (2) gives $\Delta\lambda$ = 4.9 nm. From figure 5.2 we find that our experimental results give $\Delta\lambda$ = 4.6, which is in quite good agreement with the theoretical calculations.

The a-AlN:Ti laser, we produced, is very important from biomedical applications point of view. Along with its uses in optics and photonics this laser can also be very beneficial in health sciences applications, particularly for diagnostic and therapeutic purposes. Researchers have reported that near infrared light with a wavelength between 700 nm and 900 nm has minimum absorption and the greatest penetration in body tissues (Noriyuki, Ohdan et al. 1997; Cerussi, Shah et al. 2006). Our laser produced at 780.5 nm is in this range and hence, can be used for diagnosis of deep tissues abnormality and tumors, and laser surgery of deep body tissues due to its high penetration ability in the human body.

5.2 Textiles

The deposition of amorphous AlN onto textiles was examined by Kordesch and Richardson (Kordesch and Richardson 2003). The non-woven textiles (clean room suit material) is made by thermally binding polymer threads. The threads are bound by many pads so that no loose threads are lost. The material is sensitive to heat, so that it is a good test for the successful deposition of a RE – doped Al coated textile. In this case the dopant was Tb.

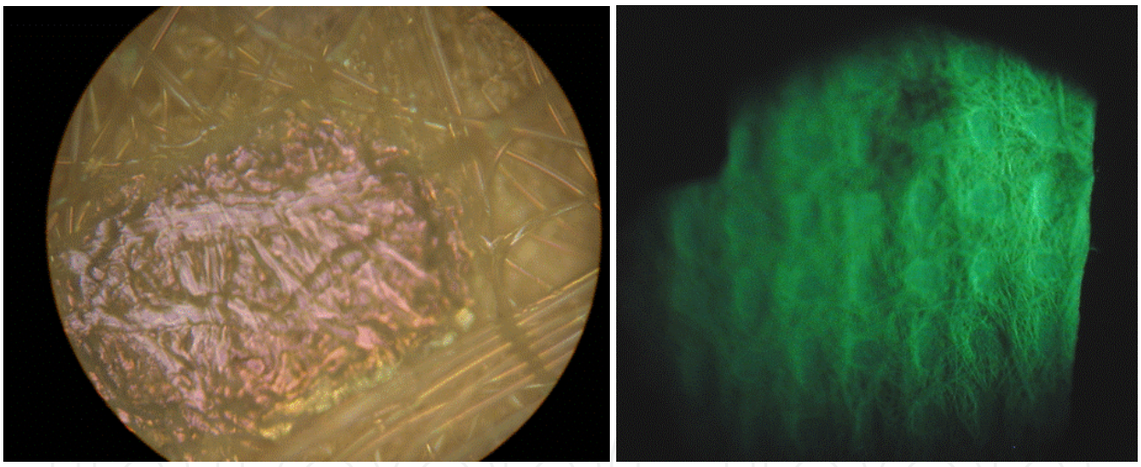

Right: Cathodoluminescence from the a-AlN:Ti coated textile. The voltage and current density used was 2.8 kV and 0.15uA/cm^2. Field of View 30mm.

Fig. 5.4. Left: a-AlN:Ti film on a thermally bonded textile pad. Field of view is 3mm.

5.3 Thermometery

A novel use of a-AlN:Ti thin films has been developed by Richardson and co-workers (Carlson, Khan et al. 2011; Wang, Carlson et al. 2011).

While the example given in Figure 5.5 is necessarily photoluminescence because the intention of the study is to determine the heating due to a gold particle in a liquid or biological environment, Er based thermometry could be used in CL and in other environments. Several other RE based thermometry systems are possible(Alden, Omrane et al.; Lai, Feng et al.).

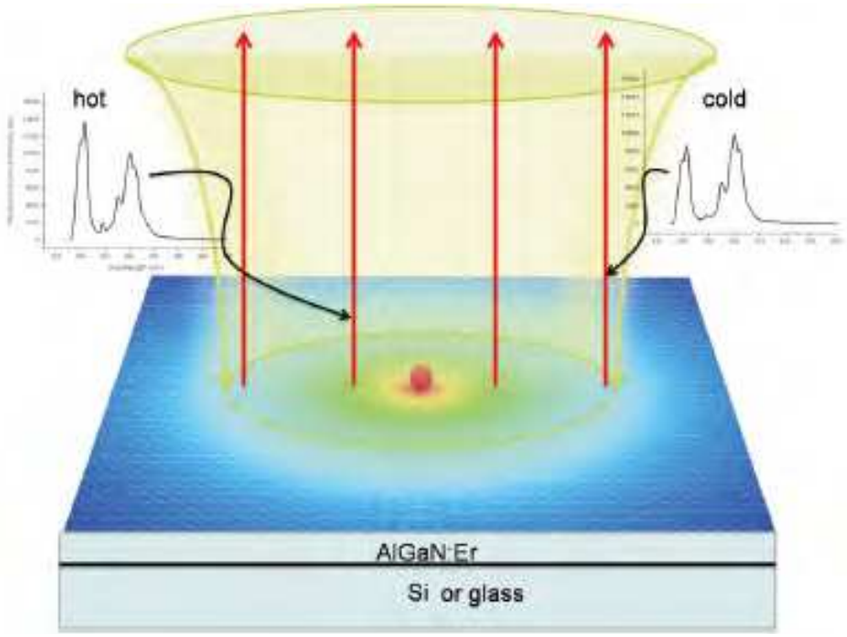

Fig. 5.5. Schematic of the Er thermometer. The Er:AlGaN film is deposited onto a substrate. The gold particle on the film surface is excited with laser light through the objective of a microscope. The photoluminescence spectrum of the Er peaks at 540 and 565 nm are used to determine the temperature of the film surrounding the substrate. From (Carlson, Khan et al. 2011), with permission.

6. Acknowledgments

We would like to thank all of the former members of our research teams who have worked on Rare Earth luminescence in the amorphous nitrides. In particular, we thank Professors Henryk J. Lozykowski, A. Ricardo Zanatta, and Hugh H. Richardson. This work was funded by several agencies, including grants from the Ballistic Missile Defence Organization and the Defence Advanced Research Projects Agency administered by the Office of Naval Research: N00014-96-1782 entitled "Growth, Doping and Contacts from Wide Band Gap Semiconductors" and grant N00014-99-1-0975 entitled "Band-Gap Engineering of the Amorphous In-Ga-Al Nitride Semiconductor Alloys for Luminescent Devices from the Ultraviolet to the Infrared."

7. References

Adachi, S. (1999). *Optical Constants of Crystalline and Semiconductors:Numerical Data and Graphical Information*, Springer.

Aldabergenova, S. B., G. Frank, et al. (2006). "Structure changes of AlN: Ho films with annealing and enhancement of the Ho3+ emission." *Journal Of Non-Crystalline Solids* 352(9-20): 1290-1293.

Aldabergenova, S. B., A. Osvet, et al. (2002). "Blue, green and red emission from Ce3+, Tb3+ and Eu3+ ions in amorphous GaN and AlN thin films." *Journal Of Non-Crystalline Solids* 299: 709-713.

Alden, M., A. Omrane, et al. "Thermographic phosphors for thermometry: A survey of combustion applications." *Progress In Energy And Combustion Science* 37(4): 422-461.

Allen S., R., H.H. and Kordesch. M.E. (2000). Luminescence of Transition and Lanthanide Metal Ions in Sputtered BN Thin Films, Ohio Univerity.

Caldwell, M. L., A. L. Martin, et al. (2001). "Emission properties of an amorphous AlN: Cr3+ thin-film phosphor." *Applied Physics Letters* 78(9): 1246-1248.

Caldwell, M. L., P. G. Van Patten, et al. (2001). "Visible luminescent activation of amorphous AlN: Eu thin-film phosphors with oxygen." *Mrs Internet Journal Of Nitride Semiconductor Research* 6(13): 1-8.

Carlson, M. T., A. Khan, et al. (2011). "Local Temperature Determination of Optically Excited Nanoparticles and Nanodots." *Nano Letters* 11(3): 1061-1069.

Cerussi, A., N. Shah, et al. (2006). "In vivo absorption, scattering, and physiologic properties of 58 malignant breast tumors determined by broadband diffuse optical spectroscopy." *Journal Of Biomedical Optics* 11(4).

Chen, H., K. Y. Chen, et al. (2000). "Band gap engineering in amorphous AlxGa1-xN: Experiment and ab initio calculations." *Applied Physics Letters* 77(8): 1117-1119.

Chen, H., K. Gurumurugan, et al. (2000). "Visible and infrared emission from GaN: Er thin films grown by sputtering." *Mrs Internet Journal Of Nitride Semiconductor Research* 5: art. no.-W3.16.

Chen, K. Y. and D. A. Drabold (2002). "First principles molecular dynamics study of amorphous AlxGa1-xN alloys." *Journal Of Applied Physics* 91(12): 9743-9751.

Dieke, G. H. (1968). *Spectra and Energy Levels of Rare Earth Ion in Crystals*. New York, Wiley.

Dierolf, V., et al., eds. (2011). *Rare-Earth Doping of Advanced Materials for Photonic Applications*.

Dimitrova, V. I., P. G. Van Patten, et al. (2001). "Photo-, cathodo-, and electroluminescence studies of sputter deposited AlN: Er thin films." *Applied Surface Science* 175: 480-483.

Dimitrova, V. I., P. G. Van Patten, et al. (2000). "Visible emission from electroluminescent devices using an amorphous AlN: Er3+ thin-film phosphor." *Applied Physics Letters* 77(4): 478-479.

Drabold, D. A. a. E., S., eds. (2010). *Theory of Defects in Semiconductors*, Springer.

Ebdah, M. (2011). Engineering the Optical, Structural, Electrial and Magnetic Properties of Oxides and Nitrides of In-Ga-Zn Thin Films Using Nanotechnology. *Physics and Astronomy*. Athens, Ohio University. PhD: 155.

Frolov, S. V., A. Fujii, et al. (1998). "Cylindrical microlasers and light emitting devices from conducting polymers." *Applied Physics Letters* 72(22): 2811-2813.

Frolov, S. V., Z. V. Vardeny, et al. (1998). "Plastic microring lasers on fibers and wires." *Applied Physics Letters* 72(15): 1802-1804.

Gedam, S. C., S. J. Dhoble, et al. (2007). "Dy3+ and Mn2+ emission in KMgSO4Cl phosphor." *Journal Of Luminescence* 124(1): 120-126.

Grinberg, M., J. Barzowska, et al. (2001). "Inhomogeneous broadening of the dominant Cr3+ sites in LiTaO3 system." *Journal Of Luminescence* 94: 85-90.

Gurumurugan, K., H. Chen, et al. (1999). "Visible cathodoluminescence of Er-doped amorphous AlN thin films." *Applied Physics Letters* 74(20): 3008-3010.

Hassan, Z. (1998). Growth, Characterizationation and Fabrication of GaN-based Device Structures. *Physics and Astronomy*. Athens, Ohio University. PhD: 1-158.

Hidalgo, P., B. Mendez, et al. (1998). "Luminescence properties of transition-metal-doped GaSb." *Physical Review B* 57(11): 6479-6484.

Housecroft, C., and Sharpe, A.G. (2007) Inorganic Chemistry (3rd Edition), Upper Saddle River, NJ, Prentic Hall.

Iacona, F., G. Franzo, et al. (2009). "Er-based materials for Si microphotonics." *Optical Materials* 31(9): 1269-1274.

Ihn, T. (2010). *Semiconductor Nanostructures: Quantum states and electronic transport*, Oxford University Press.

Jadwisienczak, W. M., H. J. Lozykowski, et al. (2000). Visible emission from AlN doped with Eu, Tb, and Er ions. *2001 Ieee International Symposium On Compound Semiconductors*: 489-494.

Jadwisienczak, W. M., H. J. Lozykowski, et al. (2000). "Luminescence of Tb ions implanted into amorphous AlN thin films grown by sputtering." *Applied Physics Letters* 76(23): 3376-3378.

Kasai, H., A. Nishikawa, et al. (2010). "Improved Eu Luminescence Properties in Eu-Doped GaN Grown on GaN Substrates by Organometallic Vapor Phase Epitaxy." *Japanese Journal Of Applied Physics* 49(4).

Kenyon A.J. and Lucarz, F. "A Critique of the Existing Model for Excitation Exchange Between Silicon Nanostructures and Erbium Ions in SIlica." from http://discovery.ucl.ac.uk/1306794.

Kenyon, A. J., C. E. Chryssou, et al. (2002). "Luminescence from erbium-doped silicon nanocrystals in silica: Excitation mechanisms." *Journal Of Applied Physics* 91(1): 367-374.

Khoshman, J. M. and M. E. Kordesch (2005). Spectroscopic ellipsometry characterization of amorphous aluminum nitride and indium nitride thin films. *Physica Status Solidi C - Conferences and Critical Reviews, Vol 2, No 7*. 2: 2821-2827.

Kik, P. G. a. P., A. (2003). *Towards the First Silicon Laser*, Kluwer Academic Publishers.

Kim, J. H. and P. H. Holloway (2004). "Room-temperature photoluminescence and electroluminescence properties of sputter-grown gallium nitride doped with europium." *Journal Of Applied Physics* 95(9): 4787-4790.

Kim, J. H., N. Shepherd, et al. (2003). "Visible and near-infrared alternating-current electroluminescence from sputter-grown GaN thin films doped with Er." *Applied Physics Letters* 83(21): 4279-4281.

Kordesch, M. E. and H. H. Richardson (2003). Electroluminescent textiles using sputter-deposited amorphous nitride-Rare-Earth ion coatings. *Electronics On Unconventional Substrates-Electrotextiles And Giant-Area Flexible Circuits*. 736: 61-66.

Kucheyev, S. O., J. S. Williams, et al. (2004). "Dynamic annealing in III-nitrides under ion bombardment." *Journal Of Applied Physics* 95(6): 3048-3054.

Lai, B. Y., L. Feng, et al. "Optical transition and upconversion luminescence in Er(3+) doped and Er(3+)-Yb(3+) co-doped fluorophosphate glasses." *Optical Materials* 32(9): 1154-1160.

Lapraz, D., P. Iacconi, et al. (1991). "Thermostimulated Luminescence And Fluorescence Of Alpha-Al2o3-Cr-3+ Samples (Ruby) - Influence Of The Cr-3+ Concentration." *Physica Status Solidi A-Applied Research* 126(2): 521-531.

Little, M. E. and M. E. Kordesch (2001). "Band-gap engineering in sputter-deposited ScxGa1-xN." *Applied Physics Letters* 78(19): 2891-2892.

Lozykowski, H. J. (1993). "Kinetics Of Luminescence Of Isoelectronic Rare-Earth Ions In Iii-V Semiconductors." *Physical Review B* 48(24): 17758-17769.

Lozykowski, H. J., W. M. Jadwisienczak, et al. (2000). "Photoluminescence and cathodoluminescence of GaN doped with Pr." *Journal Of Applied Physics* 88(1): 210-222.

MacKay, K.M., et al., (1996) Introduction to Modern Inorganic Chemistry, Boca Raton, CRC Press.

Maqbool, M. (2005). Growth Characterization and Luminescence and Optical Properties of Rare Earth elements and Transition Metals doped in Wide Gap Nitride Semiconductors. *Physics and Astronomy*. Athens, Ohio University. PhD: 1-180.

Maqbool, M. and I. Ahmad (2009). "Ultraviolet spectroscopy of Pr+3 and its use in making ultraviolet filters." *Current Applied Physics* 9(1): 234-237.

Maqbool, M., I. Ahmad, et al. (2007). "Direct ultraviolet excitation of an amorphous AlN: praseodymium phosphor by codoped Gd3+ cathodoluminescence." *Applied Physics Letters* 91(19).

Maqbool, M., G. Ali, et al. "Nanocrystals formation and intense, green emission in thermally annealed AlN:Ho films for microlaser cavities and photonic applications." *Journal Of Applied Physics* 108(4).

Maqbool, M. and T. Ali (2009). "Intense Red Catho- and Photoluminescence from 200 nm Thick Samarium Doped Amorphous AlN Thin Films." *Nanoscale Research Letters* 4(7): 748-752.

Maqbool, M., M. E. Kordesch, et al. (2009). "Electron penetration depth in amorphous AlN exploiting the luminescence of AlN:Tm/AlN:Ho bilayers." *Current Applied Physics* 9(2): 417-421.

Maqbool, M., M. E. Kordesch, et al. (2009). "Enhanced cathodoluminescence from an amorphous AlN:holmium phosphor by co-doped Gd(+3) for optical devices applications." *Journal Of The Optical Society Of America B-Optical Physics* 26(5): 998-1001.

Maqbool, M., K. Main, et al. (2010). "Titanium-doped sputter-deposited AlN infrared whispering gallery mode microlaser on optical fibers." *Optics Letters* 35(21): 3637-3639.

Maqbool, M., H. H. Richardson, et al. (2005). Cathodoluminescence of praseodymium doped AlN, GaN and turbo static BN. *GaN, AIN, InN and Their Alloys*. 831: 417-421.

Maqbool, M., H. H. Richardson, et al. (2007). "Luminescence from praseodymium doped AlN thin films deposited by RF magnetron sputtering and the effect of material structure and thermal annealing on the luminescence." *Journal Of Materials Science* 42(14): 5657-5660.

Maqbool, M., E. Wilson, et al. (2010). "Luminescence from Cr(+3)-doped AlN films deposited on optical fiber and silicon substrates for use as waveguides and laser cavities." *Applied Optics* 49(4): 653-657.

Martin, A. L., C. M. Spalding, et al. (2001). "Visible emission from amorphous AlN thin-film phosphors with Cu, Mn, or Cr." *Journal Of Vacuum Science & Technology A-Vacuum Surfaces And Films* 19(4): 1894-1897.

Masterov, V. F. and L. G. Gerchikov (1999). "Mechanisms of excitation of the f-f emission in silicon codoped with erbium and oxygen." *Semiconductors* 33(6): 616-621.

Muller, S., M. J. Zhou, et al. (2009). "Intra-shell luminescence of transition-metal-implanted zinc oxide nanowires." *Nanotechnology* 20(13).

Nishikawa, A., N. Furukawa, et al. (2010). "Improved luminescence properties of Eu-doped GaN light-emitting diodes grown by atmospheric-pressure organometallic vapor phase epitaxy." *Applied Physics Letters* 97(5).

Nishikawa, A., T. Kawasaki, et al. (2009). "Room-Temperature Red Emission from a p-Type/Europium-Doped/n-Type Gallium Nitride Light-Emitting Diode under Current Injection." *Applied Physics Express* 2(7).

Noriyuki, T., H. Ohdan, et al. (1997). "Near-infrared spectroscopic method for assessing the tissue oxygenation state of living lung." *American Journal Of Respiratory And Critical Care Medicine* 156(5): 1656-1661.

O'Donnell, K. P., ed. (2010). *Rare-Earth Doped III-Nitrides for Optoelectronic and Spintronic Applications*, Springer.

Park, J. H. and A. J. Steckl (2004). "Laser action in Eu-doped GaN thin-film cavity at room temperature." *Applied Physics Letters* 85(20): 4588-4590.

Park, J. H. and A. J. Steckl (2005). "Demonstration of a visible laser on silicon using Eu-doped GaN thin films." *Journal Of Applied Physics* 98(5).

Park, J. H. and A. J. Steckl (2006). "Visible lasing from GaN: Eu optical cavities on sapphire substrates." *Optical Materials* 28(6-7): 859-863.

Richardson, H. H., P. G. Van Patten, et al. (2002). "Thin-film electroluminescent devices grown on plastic substrates using an amorphous AlN: Tb3+ phosphor." *Applied Physics Letters* 80(12): 2207-2209.

Singh, J. a. S., K., eds. (2003). *Advances in Amorphous Semiconductors, Advances in Condensed Matter Sciences*, CRC Press.

Steckl, A. J. and R. Birkhahn (1998). "Visible emission from Er-doped GaN grown by solid source molecular beam epitaxy." *Applied Physics Letters* 73(12): 1700-1702.

Steckl, A. J. a. Z., J.M (1999). "Optoelectronic Properties and Applications of Rare Earth." *MRS Bulletin* 24: 33-38.

Street, R. A., ed. (2010). *Technology and Applications of Amorphous Silicon*, Springer.

Tessler, L. R. (1999). "Erbium in a-Si: H." *Brazilian Journal Of Physics* 29(4): 616-622.

Thurbide, K. B. and W. A. Aue (2002). "Chemiluminescent emission spectra of lead, chromium, ruthenium, iron, manganese, rhenium, osmium and tungsten in the reactive flow detector." *Spectrochimica Acta Part B-Atomic Spectroscopy* 57(5): 843-852.

Wang, D., M. T. Carlson, et al. (2011). "Absorption Cross Section and Interfacial Thermal Conductance from an Individual Optically Excited Single-Walled Carbon Nanotube." *Acs Nano* 5(9): 7391-7396.

Weingartner, R., O. Erlenbach, et al. (2006). "Thermal activation, cathodo- and photoluminescence measurements of rare earth doped (Tm, Tb, Dy, Eu, Sm, Yb) amorphous/nanocrystalline AlN thin films prepared by reactive rf-sputtering." *Optical Materials* 28(6-7): 790-793.

Wybourne B.G. and Smentek, L. (2007). *Optical Spectroscopy of Lanthanides*, CRC Press.

Zanatta, A. R., A. Khan, et al. (2007). "Red-green-blue light emission and energy transfer processes in amorphous SiN films doped with Sm and Tb." *Journal Of Physics-Condensed Matter* 19(43).

Zanatta, A. R. and L. A. O. Nunes (1998). "Green photoluminescence from Er-containing amorphous SiN thin films." *Applied Physics Letters* 72(24): 3127-3129.

Zanatta, A. R., C. T. M. Ribeiro, et al. (2001). "Visible luminescence from a-SiN films doped with Er and Sm." *Applied Physics Letters* 79(4): 488-490.

Zanatta, A. R., C. T. M. Ribeiro, et al. (2004). "Photon and electron excitation of rare-earth-doped amorphous SiN films." *Journal Of Non-Crystalline Solids* 338: 473-476.

Zanatta, A. R., C. T. M. Ribeiro, et al. (2005). "Optoelectronic and structural characteristics of Er-doped amorphous AlN films." *Journal Of Applied Physics* 98(9).

Zanatta, A. R., C. T. M. Ribeiro, et al. (2006). "Thermally synthesized ruby microstructures and luminescence centers." *Journal Of Applied Physics* 100(11).

Zanatta, A. R., H. H. Richardson, et al. (2007). "Amorphous BeN as a new solid host for rare-earth-related luminescent materials." *Physica Status Solidi-Rapid Research Letters* 1(4): 153-155.

Zegrya, G. G. and V. F. Masterov (1995). "Mechanism Of The Intensification Of F-F Luminescence In Semiconductors." *Semiconductors* 29(10): 989-995.

Zegrya, G. G. and V. F. Masterov (1996). Two novel mechanisms of f-f-luminescence resonance excitation in semiconductors. *Tenth Feofilov Symposium On Spectroscopy Of Crystals Activated By Rare-Earth And Transitional-Metal Ions*. 2706: 235-240.

Zegrya, G. G. and V. F. Masterov (1998). "Mechanism of generation of f-f radiation in semiconductor heterostructures." *Applied Physics Letters* 73(23): 3444-3446.

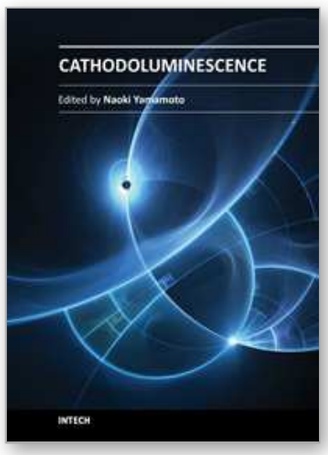

Cathodoluminescence

Edited by Dr. Naoki Yamamoto

ISBN 978-953-51-0362-2
Hard cover, 324 pages
Publisher InTech
Published online 28, March, 2012
Published in print edition March, 2012

Cathodoluminescence (CL) is a non-destructive technique to characterize optical and electronic properties of nanostructures in many kinds of materials. Major subject is to investigate basic parameters in semiconductors, impurities in oxides and phase determination of minerals. CL gives information on carrier concentration, diffusion length and life time of minority carriers in semiconductors, and impurity concentration and phase composition in composite materials. This book involves 13 chapters to present the basics in the CL technique and applications to particles, thin films and nanostructures in semiconductors, oxides and minerals. The chapters covered in this book include recent development of CL technique and applications to wide range of materials used in modern material science.

How to reference

In order to correctly reference this scholarly work, feel free to copy and paste the following:

Muhammad Maqbool, Wojciech M. Jadwisienczak and Martin E. Kordesch (2012). Cathodoluminescence from Amorphous and Nanocrystalline Nitride Thin Films Doped with Rare Earth and Transition Metals, Cathodoluminescence, Dr. Naoki Yamamoto (Ed.), ISBN: 978-953-51-0362-2, InTech, Available from: http://www.intechopen.com/books/cathodoluminescence/cathodoluminescence-from-amorphous-and-nano-crystalline-nitride-and-oxide-thin-films-doped-with-rare

INTECH
open science | open minds

InTech Europe
University Campus STeP Ri
Slavka Krautzeka 83/A
51000 Rijeka, Croatia
Phone: +385 (51) 770 447
Fax: +385 (51) 686 166
www.intechopen.com

InTech China
Unit 405, Office Block, Hotel Equatorial Shanghai
No.65, Yan An Road (West), Shanghai, 200040, China
中国上海市延安西路65号上海国际贵都大饭店办公楼405单元
Phone: +86-21-62489820
Fax: +86-21-62489821

IntechOpen